Can assimilation of crowdsourced data in hydrological modelling improve flood prediction?

M. Mazzoleni[1], M. Verlaan[2], L. Alfonso[1], M. Monego[3], D. Norbiato[3], M. Ferri[3] and D.P. Solomatine[1,4]

[1]{UNESCO-IHE Institute for Water Education, Delft, The Netherlands}

[2]{Deltares, Delft, The Netherlands}

[3]{Alto Adriatico Water Authority, Venice, Italy}

[4]{Delft University of Technology, Water Resources Section, Delft, The Netherlands}

Correspondence to: M. Mazzoleni (m.mazzoleni@unesco-ihe.org)

Abstract

Monitoring stations have been used for decades to properly measure hydrological variables and better predict floods. To this end, methods to incorporate these observations into mathematical water models have also being developed. Besides, in recent years the continued technological advances, in combination with the growing inclusion of citizens in participatory processes related to water resources management, have encouraged the increase of citizen science projects around the globe. In turn, this has stimulated the spread of low-cost sensors to allow citizens to participate in the collection of hydrological data in a more distributed way than the classic static physical sensors do. However, two main disadvantages of such crowdsourced data are the irregular availability and variable accuracy from sensor to sensor, which makes them challenging to use in hydrological modelling. This study aims to demonstrate that streamflow data, derived from crowdsourced water level observations, can improve flood prediction if integrated in hydrological models. Two different hydrological models, applied to four case studies, are considered. Realistic (albeit synthetic) time series are used to represent crowdsourced data in all case studies. In this study it is found that the data accuracies has much more influence on the model results than the irregular frequencies of data availability at which the streamflow data is assimilated. This study demonstrates that data collected by citizens,

characterised by being asynchronous and inaccurate, can still complement traditional networks formed by few accurate, static sensors and improve the accuracy of flood forecasts.

1 Introduction

Observations of hydrological variables measured by physical sensors have been increasingly integrated into mathematical models by means of model updating methods. The use of these techniques allows for the reduction of intrinsic model uncertainty and improves the flood forecasting accuracy (Todini et al., 2005). The main idea behind model updating techniques is to either update model input, states, parameters or outputs as new observations become available (Refsgaard, 1997; WMO, 1992). Input update is the classical method used in operational forecasting and uncertainties of the input data can be considered as the main source of uncertainty of the model (Bergström, 1991; Canizares et al., 1998; Todini et al., 2005). Regarding the state updating, filtering methods as Kalman filter (Kalman, 1960), extended Kalman filter (Aubert et al., 2003; Madsen and Cañizares, 1999; Verlaan, 1998), Ensemble Kalman filter (Evensen, 2006) and Particle filter (Weerts and El Serafy 2006) are the most used approaches to update a model when new observations are available.

Due to the complex nature of the hydrological processes, spatially and temporally distributed measurements are needed in the model updating procedures to ensure a proper flood prediction (Clark et al., 2008; Mazzoleni et al., 2015; Rakovec et al., 2012). However, traditional physical sensors require proper maintenance and personnel, which can be cost prohibitive for a vast network. For this reason, improvements to monitoring technology have led to the spread of low-cost sensors to measure hydrological variables, such as water level or precipitation, in a more distributed way. The main advance of using these type of sensors, defined in the paper as a "social sensor", is that they can be used not only by technicians but also by regular citizens and that due to their reduced cost and voluntary labor by citizens, result in a more spatially distributed coverage. The idea of designing these alternative networks of low-cost social sensors and using the obtained crowdsourced observations is the base of the European Project WeSenseIt (2012-2016) and various other projects that proposed to assess the usefulness of crowdsourced observations inferred by low-cost sensors owned by citizens. For instance, in the project CrowdHydrology (Lowry and Fienen, 2013), a method to monitor stream stage at designated gauging staffs using crowdsource-based text messages of water levels is developed using untrained observers. Cifelli et al. (2005) described a community-based network of

volunteers (CoCoRaHS), engaged in collecting precipitation measurements of rain, hail, and snow. An example of hydrological monitoring, established in 2009, of rainfall and streamflow values within the Andean ecosystems of Piura, Peru, based on citizen observations is reported in Célleri et al. (2009). Degrossi et al. (2013) used a network of wireless sensors in order to map the water level in two rivers passing by Sao Carlos, Brazil. Recently, the iSPUW Project was initiated to integrate data from advanced weather radar systems, innovative wireless sensors, and crowdsourcing of data via mobile applications, in order to better predict flood events the Dallas-Fort Worth Metroplex urban water systems (ISPUW, 2015; Seo et al., 2014). Other examples of crowdsourced water-related information include the so-called Crowdmap platform for collecting and communicating the information about the floods in Australia in 2011 (ABC, 2011), and informing citizens about the proper time for water supply in an intermittent water system (Alfonso, 2006; Au et al., 2000; Roy et al., 2012). Wehn et al. (2015) stressed the importance and need of public participation in water resources management to ensure citizens' involvement in the flood management cycle. Buytaert et al. (2014) provide a detailed and interesting review of the examples of citizen science applications in hydrology and water resources science. In this review paper, the potential of citizen science, based on robust, cheap, and low-maintenance sensing equipment, to complement more traditional ways of scientific data collection for hydrological sciences and water resources management is explored.

The traditional hydrological observations from physical sensors have a well-defined structure in terms of frequency and accuracy. On the other hand, crowdsourced observations are provided by citizens with varying experience of measuring environmental data and little connections between each other, and the consequence is that the low correlation between the measurements might be observed. So far, in operational hydrology practice, the added value of crowdsourced data it is not integrated into the forecasting models but only used to compare the model results with the observations in a post-event analysis. This can be related to the intrinsic variable accuracy, due to the lack of confidence in the data quality from these heterogeneous sensors, and the variable life-span of the crowdsourced observations.

Regarding data quality, Bordogna et al. (2014) and Tulloch and Szabo (2012) stated that quality control mechanisms should consider contextual conditions to deduce indicators about reliability (the expertise level of the crowd), credibility (the volunteer group), and performance of volunteers as they relate to accuracy, completeness and precision level. Bird et al. (2014) addressed the issue of data quality in conservation ecology by means of new statistical tools to

assess random error and bias. Cortes et al. (2014) evaluated data quality by distinguishing the in-situ data collected between volunteers and technicians and comparing the most frequent value reported at a given location. With in-situ exercises, it might be possible to have an indication of the reliability of data collected. However, this approach is not enough at an operational level to define accuracy in data quality. For this reason, to estimate observation accuracy in real-time, one possible approach could be to filter out the measurements following a geographic approach which defines semantic rules governing what can occur at a given location (e.g. Vandecasteele and Devillers, 2013). Another approach could be to compare measurements collected within a predefined time-window in order to calculate the most frequent value, the mean, and the standard deviation.

Crowdsourced observations can be defined as *asynchronous* because they do not have predefined rules about the arrival frequency (the observation might be taken once, occasionally or at irregular time steps, which can be smaller than the model time step) and accuracy of the measurement. In a recent paper, Mazzoleni et al. (2015) presented results of the study of the effects of distributed synthetic streamflow observations having synchronous intermittent temporal behavior and variable accuracies in a semi-distributed hydrological model. It was shown that the integration of distributed uncertain intermittent observations with single measurements coming from physical sensors would allow for the further improvements in model accuracy. However, it was not considered the possibility that the asynchronous observations might be coming at the moments not coordinated with the model time steps. A possible solution to handle asynchronous observations in time with Ensemble Kalman Filter (EnKF) is to assimilate them at the moments coinciding with the model time steps (Sakov et al., 2010). However, as these authors mention, this approach requires the disruption of the ensemble integration, the ensemble update and a restart, which may not feasible for large-scale forecasting applications. Continuous assimilation approaches, such as three-dimensional and four-dimensional variational methods (3D-Var and 4D-Var), are usually implemented in oceanographic modeling in order to integrate asynchronous observations at their corresponding arrival moments (Derber and Rosati, 1989; Huang et al., 2002; Macpherson, 1991; Ragnoli et al., 2012). In fact, oceanographic observations are commonly collected at asynchronous times. For this reason, in variational data assimilation, the past asynchronous observations are simultaneously used to minimize the cost function that measures the weighted difference between background states and observations over the time interval, and identify the best estimate of the initial state condition (Drecourt, 2004; Ide et al., 1997; Li and Navon, 2001). In addition to the 3D-Var and

4D-Var methods, Hunt et al. (2004) proposed a Four Dimensional Ensemble Kalman Filter (4DEnKF) which adapts EnKF to handle observations that have occurred at non-assimilation times. Furthermore, for linear dynamics, 4DEnKF is equivalent to the instantaneous assimilation of the measured data (Hunt et al., 2004). Similarly to 4DEnKF, Sakov et al. (2010) proposed a modification of the EnKF, the Asynchronous Ensemble Kalman Filter (AEnKF), to assimilate asynchronous observations (Rakovec et al., 2015). Contrary to the EnKF, in the AEnKF current and past observations are simultaneously assimilated at a single analysis step without the use of an adjoint model. Yet another approach to assimilate asynchronous observations in models is the so-called First-Guess at the Appropriate Time (FGAT) method. Like in 4D-Var, the FGAT compares the observations with the model at the observation time. However, in FGAT the innovations are assumed constant in time and remain the same within the assimilation window (Massart et al., 2010). In light of reviewed approaches, this study uses a pragmatic method, due in part to the linearity of the hydrological models implemented in this study, to assimilate the asynchronous crowdsourced observations.

The main objective of this study is to assess the potential use of crowdsourced data within hydrological modeling. In particular, the specific objectives of this study are a) to assess the influence of different arrival frequencies and accuracies of crowdsourced data from a single social sensor on the assimilation performances, and b) to integrate distributed low-cost social sensors with a single physical sensor to assess the improvement in the streamflow prediction in an early warning system. The methodology is applied in the Brue (UK), Sieve (Italy), Alzette (Luxemburg) and Bacchiglione (Italy) catchments, considering lumped and semi-distributed hydrological models respectively. Synthetic time series, asynchronous in time and with random accuracies, that imitate the crowdsourced data, are generated and used.

The study is organized as follows. Firstly, the case studies, the crowdsourced data and the datasets used are presented. Secondly, the hydrological models, the procedure used to integrate the crowdsourced data and the set of experiments are reported. Finally, the results, discussion, and conclusions are presented.

2 Sites locations and data

2.1 Case studies

Four different case studies are used to validate the obtained results for areas having diverse topographical and hydrometeorological features and represented by two different hydrological models. The Brue, Sieve, and Alzette catchments are considered because of the availability of precipitation and streamflow data, while the Bacchiglione catchment is one of the official case studies of the WeSenseIt Project (Huwald et al., 2013).

2.1.1 Brue catchment

The first case study is located in the Brue catchment (Figure 1), in Somerset, with a drainage area of about 135 km^2 at the catchment outlet in Lovington. The SRTM DEM of 90m resolution is used to derive the topographical characteristics, streamflow network and the consequent time of concentration, by means of the Giandotti equations (Giandotti, 1933), which is about 10 h. The hourly precipitation (49 rainfall stations) and streamflow data used in this study are supplied by the British Atmospheric Data Centre from the HYREX (Hydrological Radar Experiment) project (Moore et al., 2000; Wood et al., 2000). The average precipitation value in the catchment is estimated using the Ordinary Kriging (Matheron, 1963).

2.1.2 Sieve catchment

The second case study is the Sieve catchment (Figure 1), a tributary of the Arno River, located in the Central Italian Apennines, Italy. The catchment has a drainage area of about 822km^2 with the length of 56 km and it covers mostly hills and mountainous areas with an average elevation of 470 m above sea level. The time of concentration of the Sieve catchment is about 12 h. Hourly streamflow data are provided by the Centro Funzionale di Monitoraggio Meteo Idrologico-Idralico of the Tuscany Region at the outlet section of the catchment at Fornacina. The mean areal precipitation is calculated by Thiessen polygon method using 11 rainfall stations (Solomatine and Dulal, 2003).

2.1.3 Alzette catchment

The Alzette catchment is located in the large part of the Grand-Duchy in Luxembourg. The drainage area of the catchment is about 288 km^2 and the river has a length of 73 km along France and Luxembourg. The catchment covers cultivated land, grassland, forestland and

urbanized land (Fenicia et al., 2007). Thiessen polygon method is used for averaging the series at the individual stations and calculate hourly rainfall series (Fenicia et al., 2007), while streamflows data are available measured at the Hesperange gauging station.

2.1.4 Bacchiglione catchment

The last case study is the upstream part of the Bacchiglione River basin, located in the North-East of Italy, and tributary of the Brenta River which flows into the Adriatic Sea at the South of the Venetian Lagoon and at the North of the Po River delta. The study area has an overall extent and river length of about 400 km^2 and 50 km (Ferri et al., 2012). The main urban area located in the downstream part of the study area is Vicenza. The analysed part of the Bacchiglione River has three main tributaries. On the Western side is the confluences with the Bacchiglione are the Leogra and the Orolo Rivers, while on the Eastern side there is the Timonchio River (see Figure 2). The Alto Adriatico Water Authority (AAWA) has implemented an Early Warning System to forecast the possible future flood events.

2.2 Crowdsourced data

Social sensors can be used by citizens to provide crowdsourced distributed hydrological observations such as precipitation and water level. An example of these sensors can be a staff gauge, connected to a QR code, on which citizens can read water level indication and send observations via a mobile phone application. Another example is the collection of rainfall data via lab-generated videos (Alfonso et al., 2015). Recently, within the activities of the WeSenseIt Project (Huwald et al., 2013), one physical sensor and three staff gauges complemented by a QR code were installed in the Bacchiglione River to measure the water level. In particular, the physical sensor is located at the outlet of the Leogra catchment while the three social sensors are located at the Timonchio, Leogra and Orolo catchments outlet respectively (see Figure 2).

It is worth noting that, in most of the cases, it is difficult to directly assimilate water level observations within hydrological models. However, it is highly unrealistic to assume that citizens might observe streamflow directly. For this reason, crowdsourced *observations* of water level are used to calculate crowdsourced *data* (CSD) of streamflow, by means of rating curves assessed for the specific river location, which can be easily assimilated into hydrological models. It is because of both the uncertainty in rating curve estimation at the social sensor location and the error in the water level measurements that CSD have such low and variable accuracies when compared to streamflow data estimated from classic physical sensors. CSD is

then assimilated within mathematical models as described in Figure 3 ("Overall information flow").

In most hydrological applications, streamflow data from physical sensors are derived (and integrated into hydrological models) at a regular, synchronous, time steps. In contrast, crowdsourced water level observations are obtained by diverse type of citizens at random moments (when a citizen decides to send data). Thus, from the modeling viewpoint CSD have three main characteristics: a) irregular arrival frequency (asynchronicity); b) random accuracy; and c) random number of CSD received within two model time steps. Because streamflow CSD are not available in the case studies at the moment of this study, realistic synthetic CSD with these characteristics are generated ("Considered information flow" in Figure 3).

For the Brue, Sieve and Alzette catchments observed hourly streamflow data at the catchments outlet are interpolated to represent CSD coming at arrival frequencies higher than hourly. For the Bacchiglione catchment, synthetic hourly CSD of streamflow are calculated using measured precipitation recorded during the considered flood events (post-event simulation) as input in the hydrological model of the Bacchiglione catchment. A similar approach, termed "observing system simulation experiment" (OSSE), is commonly used in meteorology to estimate synthetic "true" states and measurements by introducing random errors in the state and measurement equations (Arnold and Dey, 1986; Errico et al., 2013; Errico and Privé, 2014). OSSEs have the advantage of making it possible to compare estimates to "true" states and they are often used for validating the data assimilation algorithms.

Further details and assumptions regarding the characteristics of CSD and related uncertainty are provided in the next sections.

2.3 Datasets

Three flood events for each one of the four described catchments are considered to assess the assimilation of CSD in hydrological modeling.

For the Brue catchment, a 2 years' time series (June 1994 to May 1996) of observed streamflow and precipitation data are available for model calibration and validation. On the other hand, for the Sieve catchment only 3 months of hourly runoff, streamflow and precipitation data (December 1959 to February 1960) are available (Solomatine and Shrestha, 2003). For the Alzette catchment, two-year hourly data (July 2000 to June 2002) are used for the model calibration and validation (Fenicia et al., 2007). For these catchments, the observed

precipitation values are treated as the “perfect forecasts” and are fed into the hydrological model.

For the Bacchiglione catchment, three flood events occurred in 2013, 2014 and 2016 are considered. In particular, the one of 2013 had high intensity and resulted in several traffic disruptions at various locations upstream Vicenza. The forecasted time series of precipitation (3-days weather forecast) is used as input to the hydrological model. In all the case studies, the observed values of streamflow at the catchment outlet (Ponte degli Angeli for the Bacchiglione) are used to assess the performance of the hydrological model.

3 Methodology

3.1 Hydrological modelling

3.1.1 Lumped model

A lumped conceptual hydrological model is implemented to estimate the streamflow hydrograph at the outlet section of the Brue, Sieve and Alzette catchments. The choice of the model is based on previous studies performed on the Brue catchment (Mazzoleni et al., 2015). Direct runoff is the input in the conceptual model and it is assessed by means of the Soil Conservation Service Curve Number method (Mazzoleni et al., 2015). The average Curve Number value within the catchment is calibrated by minimizing the difference between the simulated volume and observed quickflow, using the method proposed by Eckhardt (2005), at the outlet section.

The main module of the hydrological model is based on the Kalinin-Milyukov-Nash (KMN), Szilagyi and Szollosi-Nagy (2010), equation:

$$Q_t = \frac{1}{k} \cdot \frac{1}{(n-1)!} \int_{t_0}^{t} \left(\frac{\tau}{k} \right)^{n-1} \cdot e^{-\tau/k} \cdot I(t-\tau) \cdot \mathrm{d}\tau \qquad (1)$$

where I is the model forcing (in this case direct runoff), n (number of storage elements) and k (storage capacity expressed in hours) are the two model parameters and Q is the model output (streamflow in m^3/s). In this study, the parameter k is assumed as a linear function between the time of concentration and a coefficient c_k. The discrete state-space system of Eq. (1) derived by

Szilagyi and Szollosi-Nagy (2010) is used in this study to apply the data assimilation approach (Mazzoleni et al., 2015, 2016).

The model calibration is performed maximizing the Nash-Sutcliffe efficiency (N_{SE}) and the correlation between the simulated and observed value of streamflow, at the outlet point of the Brue, Sieve and Alzette catchments, using historical time series. The results of the calibration provided a value of the parameters n and c_k equal to 4 and 0.026, 1 and 0.0055, and 1 and 0.00064 for the Brue, Sieve, and Alzette catchments respectively.

3.1.2 Semi-distributed model

The hydrological and routing models used in this study are based on the early warning system implemented by the AAWA and described in Ferri et al. (2012). One of the goals of this study, in the framework of the WeSenseIt Project, is to test our methodology using synthetic CSD in the existing early warning system of the Bacchiglione catchment.

In the schematization of the Bacchiglione catchment, the location of physical and social sensors corresponds to the outlet section of three main sub-catchments, Timonchio, Leogra and Orolo, while the remaining sub-catchments are considered as inter-catchment. For both sub-catchments and inter-catchments, a conceptual hydrological model, described below, is used to estimate the outflow (streamflow) hydrograph. The streamflow hydrograph of the three main sub-catchments is considered as upstream boundary conditions of a routing model used to propagate the flow up to the catchment outlet (see Figure 2), while the outflow from the inter-catchment is considered as an internal boundary condition to account for their corresponding drained area. In the following, a brief description of the main components of the hydrological and routing models is provided.

The input for the hydrological model consists of precipitation only. The hydrological response of the catchment is estimated using a hydrological model that considers the routines for runoff generation and a simple routing procedure. The processes related to runoff generation (surface, sub-surface and deep flow) are modeled mathematically by applying the water balance to a control volume representative of the active soil at the sub-catchment scale. The water content S_w in the soil is updated at each calculation step dt using the following balance equation:

$$S_{w,t+dt} = S_{w,t} + P_t - R_{sur,t} - R_{sub,t} - L_t - E_{T,t} \quad (2)$$

where P and E_T are the components of precipitation and evapotranspiration, while R_{sur}, R_{sub} and L are the surface runoff, sub-surface runoff and deep percolation model states respectively (see Figure 2). The surface runoff R_{sur} is expressed by the equation based on specifying the critical threshold beyond which the mechanism of dunnian flow (saturation excess mechanism) prevails:

$$R_{sur,t} = \begin{cases} C \cdot \left(\frac{S_{w,t}}{S_{w,max}} \right) \cdot P_t \Rightarrow P_t \le f = \frac{S_{w,max} \cdot \left(S_{w,max} - S_{w,t} \right)}{\left(S_{w,max} - C \cdot S_{w,t} \right)} \\ P_t - \left(S_{w,max} - S_{w,t} \right) \Rightarrow P_t > f \end{cases}. \quad (3)$$

where C is a coefficient of soil saturation obtained by calibration, and $S_{w,max}$ is the content of water at saturation point which depends on the nature of the soil and on its use.

The sub-surface flow is considered proportional to the difference between the water content $S_{w,t}$ at time t and that at soil capacity S_c:

$$R_{sub,t} = c \cdot \left(S_{w,t} - S_c \right). \quad (4)$$

while the estimated deep flow is evaluated according to the expression proposed by Laio et al. (2001):

$$L_t = \frac{K_S}{e^{\beta \cdot \left(1 - \frac{S_c}{S_{w,max}} \right)} - 1} \cdot \left(e^{\beta \cdot \left(\frac{S_{w,t} - S_c}{S_{w,max}} \right)} - 1 \right). \quad (5)$$

where, K_S is the hydraulic conductivity of the soil in saturation conditions, β is a dimensionless exponent characteristic of the size and distribution of pores in the soil. The evaluation of the real evapotranspiration is performed assuming it as a function of the water content in the soil and potential evapotranspiration, calculated using the formulation of Hargreaves and Samani (1982).

Knowing the values of R_{sur}, R_{sub} and L, it is possible to model the surface Q_{sur}, sub-surface Q_{sub} and deep flow Q_g routed contributes according to the conceptual framework of the linear reservoir at the closing section of the single sub-catchment. In particular, in case of Q_{sur} the value of the parameter k, which is a function of the residence time in the catchment slopes, is estimated relating the velocity to the average slopes length. However, one of the challenges is to properly estimate such velocity, which should be calculated for each flood event (Rinaldo and Rodriguez-Iturbe, 1996). According to Rodríguez-Iturbe et al. (1982), this velocity is a

function of the effective rainfall intensity and the event duration. In this study, the estimation of the surface velocity is performed using the relation between velocity and intensity of rainfall excess proposed in Kumar et al. (2002), to then estimate the average travel time and the consequent parameter *k*. However, this formulation is applied in a lumped way for a given sub-catchment. As reported in McDonnell and Beven (2014), more reliable and distributed models should be used to reproduce the spatial variability of the residence times over time within the catchment. That is why, in the advanced version of the model implemented by AAWA, in each sub-catchment the runoff propagation is carried out according to the geomorphological theory of the hydrologic response. The overall catchment travel time distributions is considered as nested convolutions of statistically independent travel time distributions along sequentially connected, and objectively identified, smaller sub-catchments. The correct estimation of the residence time should be derived considering the latest findings reported in McDonnell and Beven (2014). Regarding Q_{sub} and Q_g, the value of k is calibrated comparing the observed and simulated streamflow at Vicenza.

In the early warning system implemented by AAWA in the Bacchiglione catchment, the flood propagation along the main river channel is represented by a one-dimensional hydrodynamic model, MIKE 11 (DHI, 2005). However, in order to reduce the computational time required by the analysis performed in this study, MIKE11 is replaced by a Muskingum-Cunge model (see, e.g. Todini 2007), considering rectangular river cross-sections for the estimation of hydraulic radios, wave celerities, and other hydraulic variables.

Calibration of the hydrological model parameters is performed by AAWA, and described in Ferri et al. (2012), considering the time series of precipitation from 2000 to 2010 in order to minimize the root mean square error between observed and simulated values of water level at Ponte degli Angeli gauged station. In order to stay as close as possible to the early warning system implemented by AAWA, we used the same calibrated model parameters proposed by Ferri et al. (2012).

3.2 Data assimilation procedure

3.2.1 Kalman Filter

In data assimilation, it is typically assumed that the dynamic system can be represented in the state-space as follows:

$$\mathbf{x}_t = M(\mathbf{x}_{t-1}, \vartheta, I_t) + w_t \qquad w_t \sim N(0, \mathbf{S}_t). \tag{6}$$

$$\mathbf{z}_t = H(\mathbf{x}_t, \vartheta) + v_t \qquad v_t \sim N(0, R_t). \tag{7}$$

where $\mathbf{x}_t$ and $\mathbf{x}_{t-1}$ are state vectors at time t and t-1, M is the model operator that propagates the states $\mathbf{x}$ from its previous condition to the new one as a response to the inputs I_t, while H is the operator which maps the model states into output $\mathbf{z}_t$. The system and measurements errors w_t and v_t are assumed normally distributed with zero mean and covariance $\mathbf{S}$ and R. In a hydrological modeling system, these states can represent the water stored in the soil (soil moisture, groundwater) or on the earth surface (snow pack). These states are one of the governing factors that determine the hydrograph response to the inputs into the catchment.

For the linear systems used in this study, the discrete state-space system of Eq. (1) can be represented as follows (Szilagyi and Szollosi-Nagy, 2010):

$$\mathbf{x}_t = \mathbf{\Phi}\mathbf{x}_{t-1} + \mathbf{\Gamma} I_t + w_t. \tag{8}$$

$$Q_t = \mathbf{H}\mathbf{x}_t + v_t. \tag{9}$$

where t is the time step, $\mathbf{x}$ is the vector of the model states (stored water volume in m^3), $\mathbf{\Phi}$ is the state-transition matrix (function of the model parameters n and k), $\mathbf{\Gamma}$ is the input-transition matrix and $\mathbf{H}$ is the output matrix. For example, for n=3 the matrix $\mathbf{H}$ is expressed as $\mathbf{H}=\begin{bmatrix}0 & 0 & k\end{bmatrix}$. Expressions for matrices $\mathbf{\Phi}$ and $\mathbf{\Gamma}$ can be found in Szilagyi and Szollosi-Nagy (2010).

For the Bacchiglione model (semi-distributed model), a preliminary sensitivity analysis on the model states (soil content S_w and the storage water x_{sur}, x_{sub} and x_L related to Q_{sur}, Q_{sub} and Q_g) is performed in order to decide on which of the states to update. The results of this analysis (shown in the next section) pointed out that the stored water volume x_{sur} (estimated using Eq. (8) with n=1, H=k and I_t replaced by R_{sur}) is the most sensitive state and for this reason we decided to update only this state.

The Kalman Filter (KF, Kalman, 1960) is a mathematical tool which allows estimating, in an efficient computational (recursive) way, the state of a process which is governed by a linear stochastic difference equation. KF is optimal under the assumption that the error in the process is Gaussian; in this case, KF is derived by minimizing the variance of the system error assuming that the model state estimate is unbiased.

Kalman filter procedure can be divided into two steps, namely forecast equations, (Eqs. (10) and (11)), and update (or analysis) equations (Eqs. (12), (13) and (14)):

$$\mathbf{x}_t^- = \mathbf{\Phi}\mathbf{x}_{t-1}^+ + \mathbf{\Gamma}\mathbf{I}_t . \quad (10)$$

$$\mathbf{P}_t^- = \mathbf{\Phi}\mathbf{P}_{t-1}^+\mathbf{\Phi}^{\mathrm{T}} + \mathbf{S} . \quad (11)$$

$$\mathbf{K}_t = \mathbf{P}_t^-\mathbf{H}^{\mathrm{T}}\left(\mathbf{H}\mathbf{P}_t^-\mathbf{H}^{\mathrm{T}} + R\right)^{-1} . \quad (12)$$

$$\mathbf{x}_t^+ = \mathbf{x}_t^- + \mathbf{K}_t\left(Q_t^{\mathrm{o}} - \mathbf{H}\mathbf{x}_t^-\right). \quad (13)$$

$$\mathbf{P}_t^+ = \left(\mathbf{I} - \mathbf{K}_t\mathbf{H}\right)\mathbf{P}_t^- . \quad (14)$$

where $\mathbf{K}_t$ is the Kalman gain matrix, **P** is the error covariance matrix and Q^{o} is a new observation. In this study, the observed value of streamflow Q^{o} is equal to the synthetic CSD estimated as described above. The prior model states **x** at time *t* are updated, as the response to the new available observation, using the analysis equations Eqs. (12) to (14). This allows for estimation of the values of the updated state (with superscript +) and then assessing the background estimates (with superscript –) for the next time step using the time update equations, Eqs. (10) and (11). The proper characterization of the model covariance matrix **S** is a fundamental issue in Kalman filter. In this study, in order to evaluate the effect of assimilating CSD, small values of the model error **S** are considered for each case study. In fact, a covariance matrix **S** with diagonal values of 1 m^6/s^2, 25 m^6/s^2, and 1 m^6/s^2 are considered for the Brue, Sieve, and Alzette catchments. The bigger value of **S** in the Sieve catchment is due to the higher flow magnitude in this catchment if compared to the other two. A sensitivity analysis of model performances depending on the value of **S** is reported in the Results section. For the Bacchiglione catchment, **S** is estimated, for each given flood event, as the variance between observed and simulated flow values.

3.2.2 Assimilation of crowdsourced data

As described in the previous section, a main characteristic of CSD is to be highly uncertain and asynchronous in time. Various methods have been proposed to include asynchronous observations in models. Having reviewed them, in this study we are proposing a somewhat simpler approach of Data Assimilation of Crowdsourced Observations (DACO). This method is based on the assumption that the change in the model states and in the error covariance

matrices within the two consecutive model time steps t_0 and t (observation window) is linear, while the inputs are assumed constant. All CSD received during the observation window are individually assimilated in order to update the model states and output at time t. Therefore, assuming that one CSD is available at time t_0^*, the first step of DACO (A in Figure 4) is the definition of the model states and error covariance matrix at t_0^* as:

$$\mathbf{x}_{t_0^*}^- = \mathbf{x}_{t_0}^+ + \left(\mathbf{x}_t^- - \mathbf{x}_{t_0}^+\right) \cdot \frac{t_0^* - t_0}{t - t_0} . \quad (15)$$

$$\mathbf{P}_{t_0^*}^- = \mathbf{P}_{t_0}^+ + \left(\mathbf{P}_t^- - \mathbf{P}_{t_0}^+\right) \cdot \frac{t_0^* - t_0}{t - t_0} \quad (16)$$

The second step (B in Figure 4) is the estimation of the updated model states and error covariance matrix, as the response to the streamflow CSD $Q_{t_0^*}^o$. The estimation of the posterior values of $\mathbf{x}_{t_0^*}^-$ and $\mathbf{P}_{t_0^*}^-$ is performed by Eqs. (13) and (14) respectively. The Kalman gain is estimated by Eq. (12), where the prior values of model states and error covariance matrix at t_0^* are used. Knowing the posterior value $\mathbf{x}_{t_0^*}^+$ and $\mathbf{P}_{t_0^*}^+$ it is possible to predict the value of states and covariance matrix at one model step ahead, t^* (C in Figure 4) using the model forecast equations, Eqs. (10) and (11).

The last step (D in Figure 4) is the estimation of the interpolated value of **x** and **P** at time step t. This is performed by means of a linear interpolation between the current values of **x** and **P** at t_0^* and t^*:

$$\tilde{\mathbf{x}}_t^- = \mathbf{x}_{t_0^*}^- + \left(\mathbf{x}_{t^*}^- - \mathbf{x}_{t_0^*}^+\right) \cdot \frac{t - t_0^*}{t^* - t_0^*} . \quad (17)$$

$$\tilde{\mathbf{P}}_t^- = \mathbf{P}_{t_0^*}^- + \left(\mathbf{P}_{t^*}^- - \mathbf{P}_{t_0^*}^+\right) \cdot \frac{t - t_0^*}{t^* - t_0^*} . \quad (18)$$

The symbol ~ is added on the new matrices **x** and **P** in order to differentiate them from the original forecasted values in t. Assuming that a new streamflow CSD is available at an intermediate time t_1^* (between t_0^* and t), the procedure is repeated considering the values at t_0^* and t for the linear interpolation. Then, when no more CSD are available, the updated value of $\tilde{\mathbf{x}}_t^-$ is used to predict the model states and output at t+1 (Eqs. (10) and (11)). Finally, in order to account for the intermittent behavior of this CSD, the approach proposed by Mazzoleni et al.

(2015) is applied. In this method, the model states matrix **x** is updated and forecasted when CSD are available, while without CSD the model is run using Eq. (10) and covariance matrix **P** propagated at the next time step using Eq. (11).

3.2.3 Crowdsourced data accuracy

In this section, the uncertainty related to CSD is characterized. The observational error is assumed normally distributed noise with zero mean and given standard deviation:

$$\sigma_t^Q = \alpha_t \cdot Q_t^o \tag{19}$$

where the coefficient α is related to the degree of uncertainty of the measurement (Weerts and El Serafy, 2006).

One of the main and obvious issues in citizen-based observations is to maintain the quality control of the water observations (Cortes et al., 2014; Engel and Voshell, 2002). In the Introduction section, a number of methods to estimate the model of observational uncertainty has been referred to. In this study, coefficient α is assumed a random variable uniformly distributed between 0.1 and 0.3, so we leave more thorough investigation of uncertainty level of CSD for future studies. We assumed that the maximum value of α is three times higher than the uncertainty coming from the physical sensors due to the uncertain estimation of the rating curve at the social sensor location.

3.3 Experimental setup

In this section, two sets of experiments are performed in order to test the proposed method and assess the benefit of integrating CSD, asynchronous in time and with variable accuracies, in real-time flood forecasting.

In the first set of experiments, called “Experiment 1”, assimilation of streamflow CSD at one social sensor location is carried out in the Brue, Alzette, and Sieve catchments to understand the sensitivity of the employed hydrological model - KMN - under various scenarios of these data.

In the second set of experiments, called “Experiment 2”, the distributed CSD coming from social and physical sensors, at four locations within the Bacchiglione catchment, are considered, with the aim of assessing the improvement in the flood forecasting accuracy.

3.3.1 Experiment 1: Assimilation of crowdsourced data from one social sensor

The focus of Experiment 1 is to study the performance of the hydrological model (KMN) assimilating CSD, having lower arrival frequencies than the model time step and random accuracies, coming from a social sensor located at the outlet point of the Brue, Sieve and Alzette catchments.

To analyse all possible combinations of arrival frequencies, number of CSD within the observation window (1 hour) and accuracies, a set of scenarios are considered (Figure 5), changing from regular arrival frequencies of CSD with high accuracies (scenario 1) to random and chaotic asynchronous CSD with variable accuracies (scenario 11). In each scenario, a varying number of CSD from 1 to 100 is considered. It is worth noting that for one CSD per hour and regular arrival time, scenario 1 corresponds to the case of physical sensors with observation arrival frequencies of one hour.

Scenario 2 corresponds to the case of CSD having fixed accuracies (α equal to 0.1) and irregular arrival moments, but in which at least one CSD coincides with the model time step. In particular, scenario 1 and 2 coincide for one CSD available within the observation window since it is assumed that the arrival frequencies of that CSD have to coincide with the model time step. On the other hand, the arrival frequencies of CSD in scenario 3 are assumed random and CSD might not arrive at the model time step.

Scenario 4 considers CSD with regular frequencies but random accuracies at different moments within the observation window, whereas in scenario 5 CSD have irregular arrival frequencies and random accuracies. In all the previous scenarios the arrival frequencies, the number and accuracies of CSD are assumed periodic, i.e. repeated between consecutive observation windows along all the time series. However, this periodic repetitiveness might not occur in real-life, and for this reason, a non-periodic behavior is assumed in scenarios 6, 7, 8 and 9. The non-periodicity assumptions of the arrival frequencies and accuracies are the only factors that differentiate scenarios 6, 7, 8 and 9 from the scenarios 2, 3, 4, and 5 respectively. In addition, the non-periodicity of the number of CSD within the observation window is introduced in scenario 10.

Finally, in scenario 11 CSD, in addition to all the previous characteristics, might have an intermittent behavior, i.e. not being available for one or more observation windows.

3.3.2 Experiment 2: Spatially distributed physical and social sensors

Synthetic CSD with the characteristics reported in scenarios 10 and 11 of Experiment 1 are generated due to the unavailability of streamflow CSD during this study. In order to evaluate the model performances, observed and simulated streamflows are compared, for different lead times.

Streamflow data from physical sensors are assimilated in the hydrological model of AMICO system at an hourly frequency, while CSD from social sensors are assimilated using the DACO method previously described. The updated hydrograph estimated by the hydrological model is used as the input into Muskingum-Cunge model used to propagate the streamflow downstream, to the gauged station at Ponte degli Angeli, Vicenza.

The main goal of Experiment 2 is to understand the contribution of distributed CSD to the improvement of the flood prediction at a specific point of the catchment, in this case at Ponte degli Angeli. For this reason, five different settings are introduced, and represented in Figure 6, corresponding to different types of employed sensors.

Firstly, only streamflow data from one physical sensor at the Leogra sub-catchment are assimilated to update the hydrological model of sub-catchment B (setting A). On the other hand, in setting B, CSD from the social sensor located at the Leogra sub-catchment are assimilated. In setting C, CSD from three distributed social sensors are integrated into the hydrological model. Setting D accounts for the integration of CSD from two social sensors and physical data from the physical sensor in the Leogra sub-catchment. Finally, setting E considers the complete integration between physical and social sensors in Leogra and the two social sensors in the Timonchio and Orolo sub-catchments.

4 Results

4.1 Experiment 1: Influence of crowdsourced data on flood forecasting

The observed and simulated streamflow hydrographs at the outlet section of the Brue, Sieve and Alzette catchments with and without the model update (considering hourly streamflow data) are reported in Figure 7 for nine different flood events for 1-hour lead time. As expected, it can be seen that the updated model tends to better represent the flood events than the model without updating in all the case studies. However, this improvement it is closely related to the

523 value of the matrix **S**. The higher the **S** value (uncertain model) the closer the model output gets
524 to the observation. For this reason, a sensitivity analysis on the influence of the matrix **S** on the
525 assimilation of CSD for scenario 1, i.e. coming and assimilated at regular time steps within the
526 observation windows, is reported in Figure 8. The results of Figure 8 are related to the first
527 flood event of the Brue, Sieve, and Alzette catchments. Increasing the number of CSD within
528 the observation window results in an improvement of the N_{SE} for different values of model
529 error. However, this improvement becomes negligible for a given threshold value of CSD,
530 which is a function of the considered flood event. This means that the additional CSD do not
531 add information useful for improving the model performance. Overall, increasing the value of
532 the model error **S** tends to increase N_{SE} values as mentioned before. For this reason, to better
533 evaluate the effect of assimilating CSD, a small value of **S**, i.e. model more accurate than CSD,
534 is assumed.

535 In case scenario 1, the arrival frequencies are set as regular for different model runs, so the
536 moments and accuracies in which CSD became available are always the same for any model
537 run. However, for the other scenarios, the irregular moments in which CSD becomes available
538 within the observation window and their accuracies are randomly selected and change
539 according to the different model runs. This reflects in a random model performances and
540 consequent N_{SE} values. In order to remove such random behavior, different model runs (100 in
541 this case) are carried out, assuming different random values of arrivals and accuracies
542 (coefficient α) during each model run, for a given number of CSD and lead time. The N_{SE} value
543 is estimated for each model run, so $\mu(N_{SE})$ and $\sigma(N_{SE})$ represent the mean and standard deviation
544 of the different values of N_{SE}.

545 For scenarios 2 and 3 (represented using warm, red and orange, colours in Figure 9 and Figure
546 10 for lead time equal to 24 h), the $\mu(N_{SE})$ values are smaller but comparable with the ones got
547 for scenario 1 for all the considered flood events and case studies. In particular, scenario 3 has
548 lower $\mu(N_{SE})$ than scenario 2. This can relate to the fact that both scenarios have random arrival
549 frequencies, however, in scenario 3 CSD are not provided at model time steps, as opposed to
550 scenario 2. From Figure 10, higher values of $\sigma(N_{SE})$ can be observed for scenario 3. Scenario 2
551 has the lowest standard deviation for low values of CSD because the arrival frequencies have
552 to coincide with the model time step and this stabilizes the N_{SE}. In particular, for an increasing
553 number of CSD $\sigma(N_{SE})$ tends to decrease. However, a constant trend of $\sigma(N_{SE})$ can be observed,
554 due to particular characteristics of the flood events, in case of the flood event 1 of Sieve and

555 flood event 2 and 3 of Alzette. It is worth nothing that scenario 1 has null standard deviation
556 because CSD are assumed coming at the same moments with the same accuracies for all 100
557 model runs.

558 In scenario 4, represented using blue color, CSD are considered coming at regular time steps
559 but having random accuracies. Figure 9 shows that $\mu(N_{SE})$ values are lower for scenario 4 than
560 for scenarios 2 and 3. This is related to the higher influence of CSD accuracies if compared to
561 arrival frequencies. High variability in the model performances, especially for low values of
562 CSD, it can be observed in scenario 4 (Figure 10).

563 The combined effects of random arrival frequencies and CSD accuracies is represented in
564 scenario 5 using a magenta color (i.e. the combination of warm and cold colors used for
565 scenarios 2, 3 and 4) in Figure 9 and Figure 10. As expected, this scenario has the lowest $\mu(N_{SE})$
566 and the highest $\sigma(N_{SE})$ values, compared to those reported above.

567 The remaining scenarios, from 6 to 9, are equivalent to the ones from 2 to 5 with the only
568 difference that they are non-periodic in time. For this reason, in Figure 9 and Figure 10,
569 scenarios from 6 to 9 have the same color of scenarios 2 to 5 but indicated with a dashed line
570 in order to underline their non-periodic behavior. Overall, it can be observed that non-periodic
571 scenarios have similar $\mu(N_{SE})$ values to their corresponding periodic scenario. However, the
572 smoother $\mu(N_{SE})$ trends can be explained because of the lower $\sigma(N_{SE})$ values, which means that
573 model performances are less dependent on the non-periodic nature of CSD than their period
574 behavior. Table 1 shows the N_{SE} values and model improvement obtained for the different
575 experimental scenarios during the different flood events. Small improvements are obtained
576 when N_{SE} is already high for 1 CSD as for the Sieve catchment during flood event 2 or the
577 Alzette catchment in the event 2. Moreover, it can be seen that a lower improvement is achieved
578 for scenarios (2, 3, 6 and 7) where arrival frequencies are random and accuracies fixed if
579 compared to those scenarios (4, 5, 8 and 9) where arrival frequencies are regular and accuracies
580 random.

581 In the previous analysis, model improvements are expressed only in terms of N_{SE}. However,
582 statistics such as N_{SE} only explain the overall model accuracy and not the real
583 increases/decreases in prediction error. Therefore, increases in model accuracy due to the
584 assimilation of CSD have to be presented in different ways as increased accuracy of flood peak
585 magnitudes and timing. For this reason, additional analyses are carried out to assess the change

586 in flood peak prediction considering three peaks occurred during flood event 2 in Brue
587 catchment (see Figure 7). Errors in the flood peak timing, E_{RRt}, and intensity, E_{rrI}, are estimated
588 as:

589 $$E_{RRT} = t_P^o - t_P^S . \quad (20)$$

590 $$E_{RRI} = \frac{Q_P^o - Q_P^S}{Q_P^o} . \quad (21)$$

591 where t_p^o and t_p^s are the observed and simulated peak time (h), while Q_p^o and Q_p^s are the
592 observed and simulated peak streamflow (m^3/s). From the results reported in Figure 11,
593 considering 12-h lead time, it can be observed that, overall, errors reduction in peak prediction
594 is achieved for increasing number of CSD. In particular, assimilation of CSD has more
595 influence in the reduction of the peak intensity rather than peak timing. In fact, a small reduction
596 of E_{RRT} of about 1 h is obtained even increasing the number of CSD. In both E_{RRI} and E_{RRT}, the
597 higher error reduction is obtained considering fixed CSD accuracies and random arrival
598 frequencies (e.g. scenarios 1, 2, 3, 6 and 7). In fact, smaller E_{RRI} error values are obtained for
599 scenario 1, while scenarios 5 and 9 are the ones that show the lowest improvement in terms of
600 peak prediction. These conclusions are very similar to the previous ones obtained analyzing
601 only N_{SE} as model performance measures.

602 The combination of all the previous scenarios is represented by scenario 10, where a changing
603 number of CSD in each observation windows is considered. In scenario 11 the intermittent
604 nature of CSD is accounted as well. The $\mu(N_{SE})$ and $\sigma(N_{SE})$ values of these scenarios obtained
605 for the considered flood events are showed in Figure 12. It can be observed that scenarios 10
606 tends to provide higher $\mu(N_{SE})$ and lower $\sigma(N_{SE})$ values, for a given flood event, if compared to
607 scenarios 11. In fact, intermittency in CSD tends to reduce model performance and increase the
608 variability of N_{SE} values for random configuration of arrival frequencies and CSD accuracies.
609 In particular, $\sigma(N_{SE})$ tends to be constant for increasing number of CSD.

610 **4.2 Experiment 2: Influence of distributed physical and social sensors**

611 Three different flood events occurred in the Bacchiglione catchment are used for the
612 Experiment 2. Figure 13 shows the observed and simulated streamflow value at the outlet
613 section of Vicenza. In particular, two simulated time series of streamflow are calculated using
614 as input for the hydrological model the measured and forecasted time series of precipitation.

Overall, an underestimation of the observed streamflow can be observed using forecasted input while the results achieved used measured precipitation tend to properly represent the observations. In order to find out what model states leads to a maximum increase of the model performance, a preliminary sensitivity analysis is performed. The four model states, x_S, x_{sur}, x_{sub} and x_L, related to S_w, Q_{sur}, Q_{sub} and Q_g, are uniformly perturbed by ±20% around the true state value for every time step up to the perturbation time (PT). No correlation between time steps is considered. After PT, the model realizations are run without perturbation in order to assess the effect on the system memory. No assimilation, and no states update, is performed at this step. From the results reported in Figure 14, related to the flood event 1, it can be observed that the model state x_{sur} is the most sensitive states if compared to the other ones. In addition, the perturbations of all the states seem to affect the model output even after the PT (high system memory). For this reason, in this experiment, only the model state x_{sur} is updated by means of the DACO method.

Scenarios 10 and 11, described in the previous sections, are used to represent the irregular and random behavior of CSD assimilated in the Bacchiglione catchment.

Figure 15 and Figure 16 show the results obtained from the experiment settings represented in Figure 6 during three different flood events. Three different lead time values are considered. Different model runs (100) are performed to account for the effect induced by the random arrival frequencies and accuracies of CSD within the observation window as described above. Figure 15 shows that the assimilation of streamflow from the physical sensor in the Leogra sub-catchment (setting A) provides a better streamflow prediction at Ponte degli Angeli if compared to the assimilation of a small number of CSD provided by a social sensor in the same location (setting B). In particular, Figure 15 show that, depending on the flood event, the same N_{SE} values achieved with the assimilation of physical data (hourly frequency and high accuracy) can be obtained by assimilating between 10 and 20 CSD per hour for 4 h lead time. This number of CSD tends to increase for increasing values of lead times. In case of intermittent CSD (Figure 16) the overall reduction of N_{SE} is such that even with a high number of CSD (even higher than 50 per hour) the N_{SE} is always lower than the one obtained assimilating physical streamflow data for any lead time.

For setting C, it can be observed for all three flood events that distributed social sensors in Timonchio, Leogra and Orolo sub-catchments allow for obtaining higher model performances than the one achieved with only one physical sensor (see Figure 15). However, for flood event

3 this is valid only for small lead time values. In fact, for 8 and 12 h lead time values, the contribution of CSD tend to decrease in favor of physical data from the Leogra sub-catchment. This effect is predominant for intermittent CSD, scenario 11. In this case, setting C has higher $\mu(N_{SE})$ values than setting A only during flood event 1 and for lead time values equal to 4 and 8 h (see Figure 16).

It is interesting to note that for setting D, during flood event 1, the $\mu(N_{SE})$ is higher than setting C for low number of CSD. However, with a higher number of CSD, setting C is the one providing the best model improvement for low lead time values. In the case of intermittent CSD, it can be noticed that the setting D provides always higher improvement than setting C. For flood event 1, the best model improvement is achieved for setting E, i.e. fully integrating physical sensor with distributed social sensors. On the other hand, during flood events 2 and 3, setting D shows higher improvements than setting E. For intermittent CSD the difference between setting D and E tends to reduce for all the flood events. Overall, settings D and E are the ones providing the highest $\mu(N_{SE})$ in both scenarios 10 and 11. This demonstrates the importance of integrating an existing network of physical sensors (setting A) with social sensors to improve flood predictions.

Figure 17 shows the standard deviation of the N_{SE}, $\sigma(N_{SE})$, obtained for the different settings for 4 h lead time. Similar results are obtained for the three flood events. In case of setting A, $\sigma(N_{SE})$ is equal to zero since CSD are coming from the physical sensor at regular time steps. Higher $\sigma(N_{SE})$ values are obtained for setting B, while including distributed CSD (setting C) tend to decrease the value of $\sigma(N_{SE})$. It can be observed that $\sigma(N_{SE})$ decreases for high values of CSD. As expected, the lowest values of $\sigma(N_{SE})$ are achieved including the physical sensor in the data assimilation procedure (setting D and E). Similar considerations can be drawn for intermittent CSD, where higher and more perturbed $\sigma(N_{SE})$ values are obtained.

5 Discussion

The assimilation of CSD is performed in four different case studies considering only one social sensor location in the Brue, Sieve, and Alzette catchments, and distributed social and physical sensors within the Bacchiglione catchment.

675 In the first three catchments, different characteristics of CSD are represented by means of 11
676 scenarios. Nine different flood events are used to assess the beneficial use in assimilating CSD
677 in the hydrological model to improve flood forecasting.

678 Overall, assimilation of CSD improves model performances in all the considered case studies.
679 In particular, there is a limit in the number of CSD for which satisfactory model improvements
680 can be achieved, and for which additional CSD become redundant. This asymptotic behavior,
681 when extra information is added, has also been observed using other metrics by Krstanovic and
682 Singh (1992), Ridolfi et al. (2014), Alfonso et al. (2013)), among others. From Figure 9 it can
683 be seen that, in all the considered catchments, increasing the number of model error induces an
684 increase of this asymptotic value with a consequent reduction of CSD needed to improve model
685 performances. For this reason, a small value of the model error is assumed in this study. In
686 addition, it is not possible to define a priori number of CSD needed to improve model because
687 of its different behavior for a given flood event in case of no update. In fact, as reported in Table
688 1 and Figure 8, flood events with high N_{SE} values even without update tends to achieve the
689 asymptotic values of N_{SE} for small number of CSD (e.g. flood event 1 in Brue and 2 in Sieve),
690 while more CSD are needed for flood events having low N_{SE} without update. However, for
691 these case studies and during these nine flood events, an indicative value of 10 CSD can be
692 considered to achieve a good model improvement.

693 Figure 9 and Figure 10 show the $\mu(N_{SE})$ and $\sigma(N_{SE})$ values for the scenarios 2 to 9. Figure 9
694 demonstrate that for irregular arrival frequencies and constant accuracies (e.g. scenarios 2, 3, 6
695 and 7) the N_{SE} is higher than for scenarios in which accuracies are variable and arrival
696 frequencies fixed (e.g. scenarios 4, 5, 8 and 9). These results point out that the model
697 performance is more sensitive to the accuracies of CSD than to the moments in time at which
698 the streamflow CSD become available. Overall, $\sigma(N_{SE})$ tends to decrease for high number of
699 CSD. The combined effects of irregular frequencies and uncertainties are reflected in scenario
700 5, which has lower mean and higher standard deviation of N_{SE} if compared to the first four
701 scenarios.

702 An interesting fact is that, passing from periodic to non-periodic scenarios, the standard
703 deviation $\sigma(N_{SE})$ is significantly reduced, while $\mu(N_{SE})$ remains the same but with a smoother
704 trend. A non-periodic behavior of CSD, common in real life, helps to reduce the fluctuation of
705 the N_{SE} generated by the random behavior of streamflow CSD. Finally, the results obtained for
706 scenarios 10 and 11 are showed in Figure 12. The assimilation of irregular number of CSD in

scenario 10, in each observation window, seems to provide the similar $\mu(N_{SE})$ than the ones obtained with scenario 9. One of the main outcomes is that the intermittent nature of CSD (scenario 11) induces a drastic reduction of the N_{SE} and an increase in its noise in both considered flood events. All these previous results are consistent across the considered catchments.

In the case of the Bacchiglione catchment, the data from physical and social sensors are assimilated within a hydrological model to improve the poor flow prediction in Vicenza for the three considered flood events. In fact, these predictions are affected by an underestimation of the 3-days rainfall forecast used as input in flood forecasting practice in this area.

One of the main outcomes of these analyses is that the replacement of a physical sensor (setting A) for a social sensor at only one location (settings B) does not improve the model performance in terms of N_{SE} for a small number of CSD. Figure 15 and Figure 16 show that distributed locations of social sensors (setting C) can provide higher values of N_{SE} than a single physical sensor, even for a low number of CSD, in case of CSD having the characteristic of scenario 10. For flood event 1, setting C provides better model improvement than setting D for low lead time values and high number of CSD. This can be due to the fact that the physical sensor at Leogra provides constant improvement, for a given lead time, while the social sensor tends to achieve better results with a higher number of CSD. This dominant effect of the social sensor, for high number of CSD, tends to increase for the higher lead times. On the other hand, for intermittent CSD (scenario 11) this effect decreases in particular for flood events 2 and 3.

Integrating physical and social sensors (setting D and E) induces the highest model improvements for all the three flood events. For flood event 1, assimilation from setting E it appears to provide better results than assimilation from setting D. Opposite results are obtained for flood events 2 and 3. In fact, the high $\mu(N_{SE})$ values of setting D can be due to the fact that flood events 2 and 3 are characterized by one main peak and similar shape while flood event 1 has two main peaks. Assimilation of CSD from distributed social sensors tends to reduce the variability of the N_{SE} coefficient in both scenarios 10 and 11.

6 Conclusions

This study assesses the potential use of crowdsourced data in hydrological modeling, which are characterized by irregular availability and variable accuracy. We demonstrate that even data with these characteristics can improve flood prediction if integrated into hydrological models.

738 This opens new opportunities in terms of exploiting data being collected in current citizen
739 science projects for the modeling exercise. Our results do not support the idea that social-
740 sensors should partially or totally replace the existing network of physical sensors; instead, that
741 these new data should be used to compensate the lack of traditional observations. In fact, in
742 case of a dense network of physical sensors, the additional information from social sensors
743 might not be necessary because of the high accuracy of the hydrological observations derided
744 by physical sensors

745 Four different case studies, the Brue (UK), Sieve (Italy), Alzette (Luxemburg) and Bacchiglione
746 (Italy) catchments are considered, and the two types of hydrological models are used. In the
747 Experiment 1 (Brue, Sieve and Alzette catchments) the sensitivity of the model results to the
748 assimilation of crowdsourced data, having different frequencies and accuracies, derived from a
749 hypothetical social sensor at the catchments outlet is assessed. On the other hand, in the
750 Experiment 2 (Bacchiglione catchment), the influence of the combined assimilation of
751 crowdsourced data, from a distributed network of social sensors, and existing streamflow data
752 from physical sensors is evaluated. Because crowdsourced streamflow data are not yet available
753 in all case studies, realistic synthetic data with various characteristics of arrival frequencies and
754 accuracies are introduced.

755 Overall, we demonstrated that results are very similar in terms of model behavior assimilating
756 asynchronous data in all case studies.

757 In Experiment 1, it is found that increasing the number of crowdsourced data within the
758 observation window increases the model performance even if these data have irregular arrival
759 frequencies and accuracies. Moreover, data accuracy affects the average value of N_{SE} more than
760 the moment in which these data are assimilated. The noise in the N_{SE} is reduced when the
761 assimilated data are considered having non-periodic behavior. In addition, the intermittent
762 nature of the data tends to drastically reduce the N_{SE} of the model for different values of lead
763 times. In fact, if the intervals between the data are too large then the abundance of crowdsourced
764 data at other times and places is no longer able to compensate their intermittency.

765 Experiment 2 showed that, in the Bacchiglione catchment, the integration of data from social
766 sensors and a single physical sensor could improve the flood prediction even for a small number
767 of intermittent crowdsourced data. In case of both physical and social sensors located at the
768 same place, the assimilation of physical data gives the same model improvement than the
769 assimilation of high number and non-intermittent behavior of crowdsourced data. Overall, the

integration of existing physical sensors with a new network of social sensors can improve the model predictions. Although the cases and models are different, the presented study demonstrated that the results obtained are very similar in terms of model behavior assimilating asynchronous data.

Although we have obtained interesting results, this work has some limitations. Firstly, the proposed method used to assimilate crowdsourced data is applied to the linear parts of hydrological models. This means that the proposed methodology has to be tested on models with non-linear dynamics. Secondly, while realistic synthetic streamflow data are used in this study, the developed methodology is not tested with data coming from actual social sensors. Therefore, the conclusions need to be confirmed using real crowdsourced observations of water level. Finally, advancing methods for a more accurate assessment of the data quality and accuracy of data derived from social sensors need to be considered (e.g. developing a pre-filtering module aimed to select only data having good accuracy while discarding the one with low accuracy).

Future work will be aimed to address the limitations formulated above, which will allow for a better characterization of the crowdsourced data, making them a reliable data source for model-based forecasting.

Acknowledgements

This research was partly funded in the framework of the EC FP7 Project WeSenseIt: Citizen Observatory of Water, grant agreement No. 308429. Data used were supplied by the British Atmospheric Data Centre from the NERC Hydrological Radar Experiment Dataset http://www.badc.rl.ac.uk/data/hyrex/ and by the Alto Adriatico Water Authority (Italy). The Authors wish to thank the Editor and two anonymous reviewers for their insightful and useful comments.

References

ABC: ABC's crowdsourced flood-mapping initiative, ABCs Crowdsourced Flood-Mapp. Initiat. [online] Available from: http://www.abc.net.au/technology/articles/2011/01/13/3112261.htm (Accessed 20 January 2016), 2011.

Alberoni, P., Collier, C. and Khabiti, R.: ACTIF Best practice paper - Understanding and reducing uncertainty in flood forecasting, Proceeding Act. Conf., (1), 1–43, 2005.

Alfonso, L.: Use of hydroinformatics technologies for real time water quality management and operation of distribution networks. Case study of Villavicencio, Colombia, M.Sc. Thesis, UNESCO-IHE, Institute for Water Education, Delft, The Netherlands., 2006.

Alfonso, L., He, L., Lobbrecht, A. and Price, R.: Information theory applied to evaluate the discharge monitoring network of the Magdalena River, J. Hydroinformatics, 15(1), 211, doi:10.2166/hydro.2012.066, 2013.

Alfonso, L., Chacon, J. and Pena-Castellanos. G.: Allowing Citizens to Effortlessly Become Rainfall Sensors, in 36th IAHR World Congress edited, The Hague, the Netherlands, 2015.

Arnold, C. P. and Dey, C. H.: Observing-Systems Simulation Experiments: Past, Present, and Future, Bull. Am. Meteorol. Soc., 67(6), 687–695, doi:10.1175/1520-0477(1986)067<0687:OSSEPP>2.0.CO;2, 1986.

Au, J., Bagchi, P., Chen, B., Martinez, R., Dudley, S. A. and Sorger, G. J.: Methodology for public monitoring of total coliforms, Escherichia coli and toxicity in waterways by Canadian high school students, J. Environ. Manage., 58(3), 213–230, doi:10.1006/jema.2000.0323, 2000.

Aubert, D., Loumagne, C. and Oudin, L.: Sequential assimilation of soil moisture and streamflow data in a conceptual rainfall–runoff model, J. Hydrol., 280(1–4), 145–161, doi:10.1016/S0022-1694(03)00229-4, 2003.

Bergström, S.: Principles and confidence in hydrological modelling, Hydrol. Res., 22(2), 123–136, 1991.

Bird, T. J., Bates, A. E., Lefcheck, J. S., Hill, N. A., Thomson, R. J., Edgar, G. J., Stuart-Smith, R. D., Wotherspoon, S., Krkosek, M., Stuart-Smith, J. F., Pecl, G. T., Barrett, N. and Frusher, S.: Statistical solutions for error and bias in global citizen science datasets, Biol. Conserv., 173, 144–154, doi:10.1016/j.biocon.2013.07.037, 2014.

826 Bordogna, G., Carrara, P., Criscuolo, L., Pepe, M. and Rampini, A.: A linguistic decision
827 making approach to assess the quality of volunteer geographic information for citizen
828 science, Inf. Sci., 258, 312–327, doi:10.1016/j.ins.2013.07.013, 2014.
829 Buytaert, W., Zulkafli, Z., Grainger, S., Acosta, L., Alemie, T. C., Bastiaensen, J., De BiÃ¨vre,
830 B., Bhusal, J., Clark, J., Dewulf, A., Foggin, M., Hannah, D. M., Hergarten, C., Isaeva, A.,
831 Karpouzoglou, T., Pandeya, B., Paudel, D., Sharma, K., Steenhuis, T., Tilahun, S., Van
832 Hecken, G. and Zhumanova, M.: Citizen science in hydrology and water resources:
833 opportunities for knowledge generation, ecosystem service management, and sustainable
834 development, Front. Earth Sci., 2(October), 1–21, doi:10.3389/feart.2014.00026, 2014.
835 Canizares, R., Heemink, A. W. and Vested, H. J.: Application of advanced data assimilation
836 methods for the initialisation of storm surge models, J. Hydraul. Res., 36(4), 655–674,
837 doi:10.1080/00221689809498614, 1998.
838 Célleri, R., Buytaert, W., De Bièvre, B., Tobón, C., Crespo, P., Molina, J. and Feyen, J.:
839 Understanding the hydrology of tropical Andean ecosystems through an Andean Network
840 of Basins, [online] Available from: http://dspace.ucuenca.edu.ec/handle/123456789/22089
841 (Accessed 19 February 2016), 2009.
842 Cifelli, R., Doesken, N., Kennedy, P., Carey, L. D., Rutledge, S. A., Gimmestad, C. and Depue,
843 T.: The Community Collaborative Rain, Hail, and Snow Network: Informal Education for
844 Scientists and Citizens, Bull. Am. Meteorol. Soc., 86(8), 1069–1077, 2005.
845 Clark, M. P., Rupp, D. E., Woods, R. A., Zheng, X., Ibbitt, R. P., Slater, A. G., Schmidt, J. and
846 Uddstrom, M. J.: Hydrological data assimilation with the ensemble Kalman filter: Use of
847 streamflow observations to update states in a distributed hydrological model, Adv. Water
848 Resour., 31(10), 1309–1324, doi:10.1016/j.advwatres.2008.06.005, 2008.
849 Cortes Arevalo, V. J., Charrière, M., Bossi, G., Frigerio, S., Schenato, L., Bogaard, T.,
850 Bianchizza, C., Pasuto, A. and Sterlacchini, S.: Evaluating data quality collected by
851 volunteers for first-level inspection of hydraulic structures in mountain catchments, Nat.
852 Hazards Earth Syst. Sci., 14(10), 2681–2698, doi:10.5194/nhess-14-2681-2014, 2014.
853 Degrossi, L. C., Do Amaral, G. G., da Vasconcelos, E. S. M., Albuquerque, J. P. and Ueyama,
854 J.: Using Wireless Sensor Networks in the Sensor Web for Flood Monitoring in Brazil, in
855 Proceedings of the 10th International ISCRAM Conference, Baden-Baden, Germany.
856 [online] Available from:
857 http://humanitariancomp.referata.com/wiki/Using_Wireless_Sensor_Networks_in_the_Sen
858 sor_Web_for_Flood_Monitoring_in_Brazil (Accessed 10 February 2016), 2013.

Derber, J. and Rosati, A.: A Global Oceanic Data Assimilation System, J. Phys. Oceanogr., 19(9), 1333–1347, doi:10.1175/1520-0485(1989)019<1333:AGODAS>2.0.CO;2, 1989.

DHI: MIKE FLOOD User Manual, 2005.

Drecourt, J.-P.: Data assimilation in hydrological modelling, Environment & Resources DTU. Technical University of Denmark., 2004.

Eckhardt, K.: How to construct recursive digital filters for baseflow separation, Hydrol. Process., 19(2), 507–515, doi:10.1002/hyp.5675, 2005.

Engel, S. R. and Voshell Jr, J. R.: Volunteer biological monitoring: can it accurately assess the ecological condition of streams?, Am. Entomol., 48(3), 164–177, 2002.

Errico, R. M. and Privé, N. C.: An estimate of some analysis-error statistics using the Global Modeling and Assimilation Office observing-system simulation framework, Q. J. R. Meteorol. Soc., 140(680), 1005–1012, doi:10.1002/qj.2180, 2014.

Errico, R. M., Yang, R., Privé, N. C., Tai, K.-S., Todling, R., Sienkiewicz, M. E. and Guo, J.: Development and validation of observing-system simulation experiments at NASA's Global Modeling and Assimilation Office, Q. J. R. Meteorol. Soc., 139(674), 1162–1178, doi:10.1002/qj.2027, 2013.

Evensen, G.: Data Assimilation: The Ensemble Kalman Filter, 2nd ed. 2009 edition., Springer, Place of publication not identified., 2006.

Fenicia, F., Solomatine, D. P., Savenije, H. H. G. and Matgen, P.: Soft combination of local models in a multi-objective framework, Hydrol. Earth Syst. Sci. Discuss., 4, 91–123, doi:10.5194/hessd-4-91-2007, 2007.

Ferri, M., Monego, M., Norbiato, D., Baruffi, F., Toffolon, C. and Casarin, R.: La piattaforma previsionale per i bacini idrografici del Nord Est Adriatico (I), in Proc.XXXIII Conference of Hydraulics and Hydraulic Engineering, p. 10, Brescia., 2012.

Giandotti, M.: Previsione delle piene e delle magre dei corsi d'acqua, Servizio Idrografico Italiano, Rome., 1933.

Hargreaves, G.H. and Samani, Z.A.: Estimating potential evapotranspiration, J. Irrig. Drain. Div., 108(3), 225–230, 1982.

Huang, B., Kinter, J. L. and Schopf, P. S.: Ocean data assimilation using intermittent analyses and continuous model error correction, Adv. Atmospheric Sci., 19(6), 965–992, doi:10.1007/s00376-002-0059-z, 2002.

Hunt, B. R., Kalnay, E., Kostelich, E. J., Ott, E., Patil, D. J., Sauer, T., Szunyogh, I., Yorke, J. A. and Zimin, A. V.: Four-dimensional Ensemble Kalman Filtering, Tellus A, 56(4), 273–277, doi:10.1111/j.1600-0870.2004.00066.x, 2004.

Huwald, H., Barrenetxea, G., de Jong, S., Ferri, M., Carvalho, R., Lanfranchi, V., McCarthy, S., Glorioso, G., Prior, S., Solà, E., Gil-Roldàn, E., Alfonso, L., Wehn de Montalvo, U., Onencan, A., Solomatine, D. and Lobbrecht, A.: D1.11 Sensor technology requirement analysis, Confidential Deliverable, The WeSenseIt Project (FP7/2007-2013 grant agreement no 308429)., 2013.

Ide, K., Courtier, P., Ghil, M. and Lorenc, A. C.: Unifed notation for data assimilation: operational, sequential and variational, J. Meteorol. Soc. Jpn., 75(1B), 181–189, 1997.

ISPUW: iSPUW: Integrated Sensing and Prediction of Urban Water for Sustainable Cities, [online] Available from: http://ispuw.uta.edu/nsf/ (Accessed 19 February 2016), 2015.

Kalman, R. E.: A new approach to linear filtering and prediction problems, J. Basic Eng., 82(1), 35–45, doi:10.1115/1.3662552, 1960.

Krstanovic, P. F. and Singh, V. P.: Evaluation of rainfall networks using entropy: II. Application, Water Resour. Manag., 6(4), 295–314, doi:10.1007/BF00872282, 1992.

Kumar, R., Chatterjee, C., Lohani, A. K., Kumar, S. and Singh, R. D.: Sensitivity Analysis of the GIUH based Clark Model for a Catchment, Water Resour. Manag., 16(4), 263–278, doi:10.1023/A:1021920717410, 2002.

Laio, F., Porporato, A., Ridolfi, L. and Rodriguez-Iturbe, I.: Plants in water-controlled ecosystems: active role in hydrologic processes and response to water stress: II. Probabilistic soil moisture dynamics, Adv. Water Resour., 24(7), 707–723, doi:10.1016/S0309-1708(01)00005-7, 2001.

Li, Z. and Navon, I. M.: Optimality of variational data assimilation and its relationship with the Kalman filter and smoother, Q. J. R. Meteorol. Soc., 127(572), 661–683, doi:10.1002/qj.49712757220, 2001.

Lowry, C. S. and Fienen, M. N.: CrowdHydrology: Crowdsourcing hydrologic data and engaging citizen scientists, GroundWater, 51(1), 151–156, doi:10.1111/j.1745-6584.2012.00956.x, 2013.

Macpherson, B.: Dynamic initialization by repeated insertion of data, Q. J. R. Meteorol. Soc., 117(501), 965–991, doi:10.1002/qj.49711750105, 1991.

Madsen, H. and Cañizares, R.: Comparison of extended and ensemble Kalman filters for data assimilation in coastal area modelling, Int. J. Numer. Methods Fluids, 31(6), 961–981, doi:10.1002/(SICI)1097-0363(19991130)31:6<961::AID-FLD907>3.0.CO;2-0, 1999.

Massart, S., Pajot, B., Piacentini, A. and Pannekoucke, O.: On the merits of using a 3D-FGAT assimilation scheme with an outer loop for atmospheric situations governed by transport, Mon. Weather Rev., 138(12), 4509–4522, 2010.

Matheron, G.: Principles of geostatistics, Econ. Geol., 58(8), 1246–1266, 1963.

Mazzoleni, M., Alfonso, L. and Solomatine, D.: Influence of spatial distribution of sensors and observation accuracy on the assimilation of distributed streamflow data in hydrological modelling, Hydrological Science Journal, doi: 10.1080/02626667.2016.1247211, 2016.

Mazzoleni, M., Alfonso, L., Chacon-Hurtado, J. and Solomatine, D.: Assimilating uncertain, dynamic and intermittent streamflow observations in hydrological models, Adv. Water Resour., 83, 323–339, 2015.

McDonnell, J. J. and Beven, K.: Debates—The future of hydrological sciences: A (common) path forward? A call to action aimed at understanding velocities, celerities and residence time distributions of the headwater hydrograph, Water Resour. Res., 50(6), 5342–5350, doi:10.1002/2013WR015141, 2014.

Moore, R. J., Jones, D. A., Cox, D. R. and Isham, V. S.: Design of the HYREX raingauge network, Hydrol. Earth Syst. Sci., 4(4), 521–530, doi:10.5194/hess-4-521-2000, 2000.

Ragnoli, E., Zhuk, S., Donncha, F. O., Suits, F. and Hartnett, M.: An optimal interpolation scheme for assimilation of HF radar current data into a numerical ocean model, in Oceans, 2012, pp. 1–5., 2012.

Rakovec, O., Weerts, A. H., Hazenberg, P., F. Torfs, P. J. J. and Uijlenhoet, R.: State updating of a distributed hydrological model with ensemble kalman Filtering: Effects of updating frequency and observation network density on forecast accuracy, Hydrol. Earth Syst. Sci., 16(9), 3435–3449, doi:10.5194/hess-16-3435-2012, 2012.

Rakovec, O., Weerts, A. H., Sumihar, J. and Uijlenhoet, R.: Operational aspects of asynchronous filtering for flood forecasting, Hydrol. Earth Syst. Sci., 19(6), 2911–2924, doi:10.5194/hess-19-2911-2015, 2015.

Refsgaard, J. C.: Validation and Intercomparison of Different Updating Procedures for Real-Time Forecasting, Nord. Hydrol., 28(2), 65–84, doi:10.2166/nh.1997.005, 1997.

952 Ridolfi, E., Alfonso, L., Baldassarre, G. D., Dottori, F., Russo, F. and Napolitano, F.: An
953 entropy approach for the optimization of cross-section spacing for river modelling, Hydrol.
954 Sci. J., 59(1), 126–137, doi:10.1080/02626667.2013.822640, 2014.
955 Rinaldo, A. and Rodriguez-Iturbe, I.: Geomorphological Theory of the Hydrological Response,
956 Hydrol. Process., 10(6), 803–829, doi:10.1002/(SICI)1099-1085(199606)10:6<803::AID-
957 HYP373>3.0.CO;2-N, 1996.
958 Rodríguez-Iturbe, I., González-Sanabria, M. and Bras, R. L.: A geomorphoclimatic theory of
959 the instantaneous unit hydrograph, Water Resour. Res., 18(4), 877–886,
960 doi:10.1029/WR018i004p00877, 1982.
961 Roy, H. E., Pocock, M. J. O., Preston, C. D., Roy, D. B. and Savage, J.: Understanding Citizen
962 Science and Environmental Monitoring, Final Report of UK Environmental Observation
963 Framework., 2012.
964 Sakov, P., Evensen, G. and Bertino, L.: Asynchronous data assimilation with the EnKF, Tellus
965 A, 62(1), 24–29, doi:10.1111/j.1600-0870.2009.00417.x, 2010.
966 Seo, D. ., Kerke, B., Zink, M., Fang, N., Gao, J. and Yu, X.: iSPUW: A Vision for Integrated
967 Sensing and Prediction of Urban Water for Sustainable Cities., 2014.
968 Solomatine, D. P. and Dulal, K. N.: Model trees as an alternative to neural networks in
969 rainfall—runoff modelling, Hydrol. Sci. J., 48(3), 399–411,
970 doi:10.1623/hysj.48.3.399.45291, 2003.
971 Szilagyi, J. and Szollosi-Nagy, A.: Recursive Streamflow Forecasting: A State Space Approach
972 - CRC Press Book., 2010.
973 Todini, E.: A mass conservative and water storage consistent variable parameter Muskingum-
974 Cunge approach, Hydrol. Earth Syst. Sci., 11, 1645–1659, 2007.
975 Tulloch, A. I. T. and Szabo, J. K.: A behavioural ecology approach to understand volunteer
976 surveying for citizen science datasets, Emu, 112(4), 313, doi:10.1071/MU12009, 2012.
977 Vandecasteele, A. and Devillers, R.: Improving volunteered geographic data quality using
978 semantic similarity measurements, ISPRS-Int. Arch. Photogramm. Remote Sens. Spat. Inf.
979 Sci., 1(1), 143–148, 2013.
980 Verlaan, M.: Efficient Kalman Filtering Algorithms for Hydrodynamic Models, PhD Thesis,
981 Delft University of Technology, The Netherlands., 1998.
982 Weerts, A. H. and El Serafy, G. Y. H.: Particle filtering and ensemble Kalman filtering for state
983 updating with hydrological conceptual rainfall-runoff models, Water Resour. Res., 42(9), 1–
984 17, doi:10.1029/2005WR004093, 2006.

Wehn, U., Rusca, M., Evers, J. and Lanfranchi, V.: Participation in flood risk management and the potential of citizen observatories: A governance analysis, Environmental Science & Policy, 48, 225-236, 2015

WMO: Simulated real-time intercomparison of hydrological models, World Meteorological Organization., 1992.

Wood, S. J., Jones, D. A. and Moore, R. J.: Accuracy of rainfall measurement for scales of hydrological interest, Hydrol. Earth Syst. Sci. Discuss., 4(4), 531–543, 2000.

994 **Tables**

995

996 Table 1. N_{SE} improvements (%), from 1 to 50 CSD, for different experimental scenarios during
997 the nine flood events occurred in the Brue, Sieve and Alzette catchments.

Scenario	1	2	3	4	5	6	7	8	9
Brue - event 1	0.126	0.125	0.140	0.243	0.253	0.125	0.144	0.237	0.248
Brue - event 2	0.416	0.413	0.445	0.920	0.902	0.413	0.463	0.841	0.870
Brue - event 3	0.443	0.438	0.472	0.890	0.842	0.440	0.471	0.809	0.822
Sieve - event 1	0.250	0.246	0.228	0.271	0.221	0.247	0.225	0.263	0.237
Sieve - event 2	0.066	0.064	0.067	0.057	0.056	0.064	0.068	0.057	0.060
Sieve - event 3	0.629	0.623	0.632	1.085	1.045	0.625	0.634	1.019	0.995
Alzette - event 1	0.884	0.881	0.883	1.274	1.265	0.882	0.890	1.251	1.342
Alzette - event 2	0.137	0.135	0.135	0.120	0.121	0.134	0.147	0.119	0.135
Alzette - event 3	0.314	0.309	0.305	0.297	0.283	0.310	0.315	0.297	0.281

998

Figures

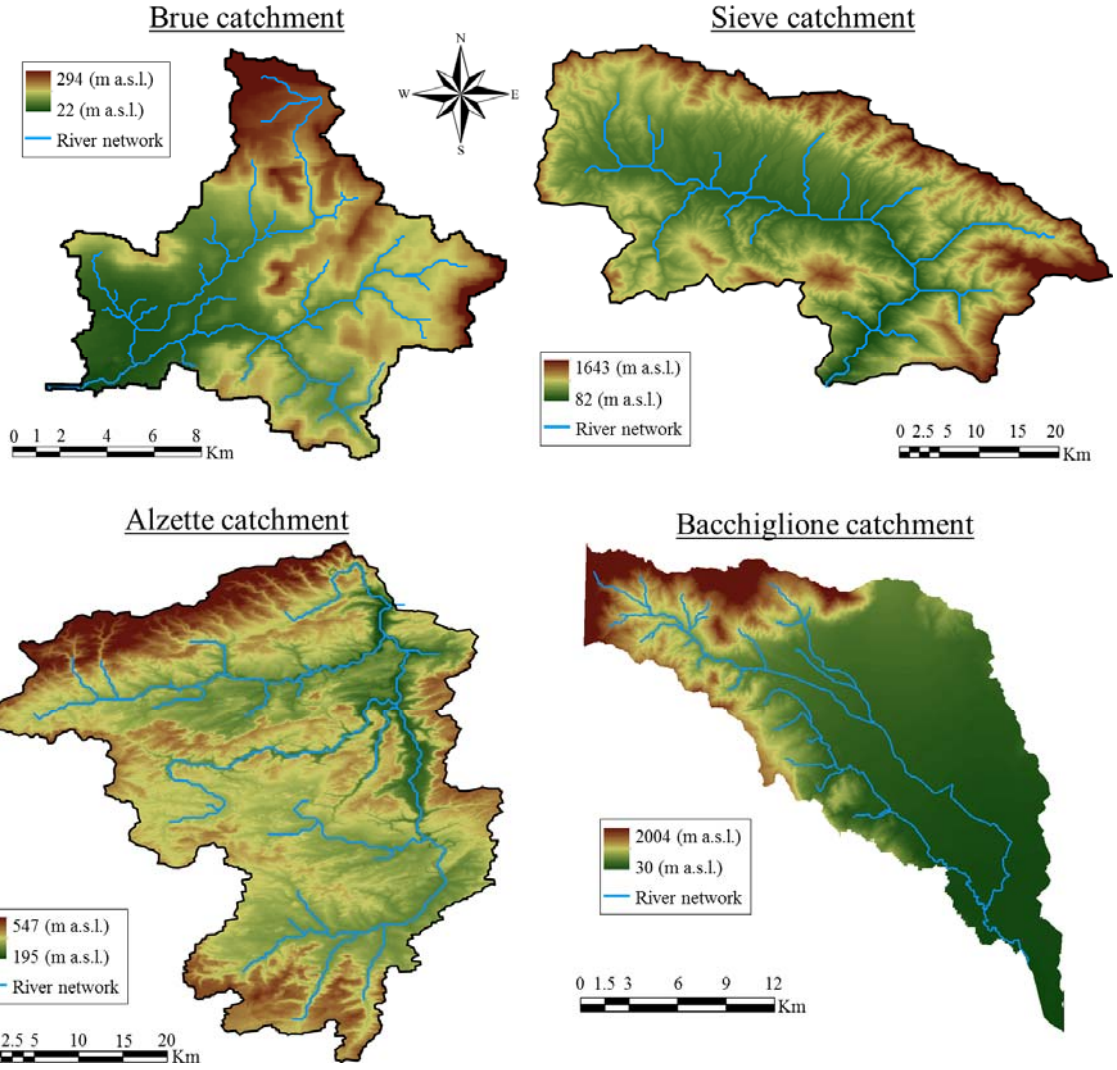

Figure 1. Representation of the four case studies considered in this study

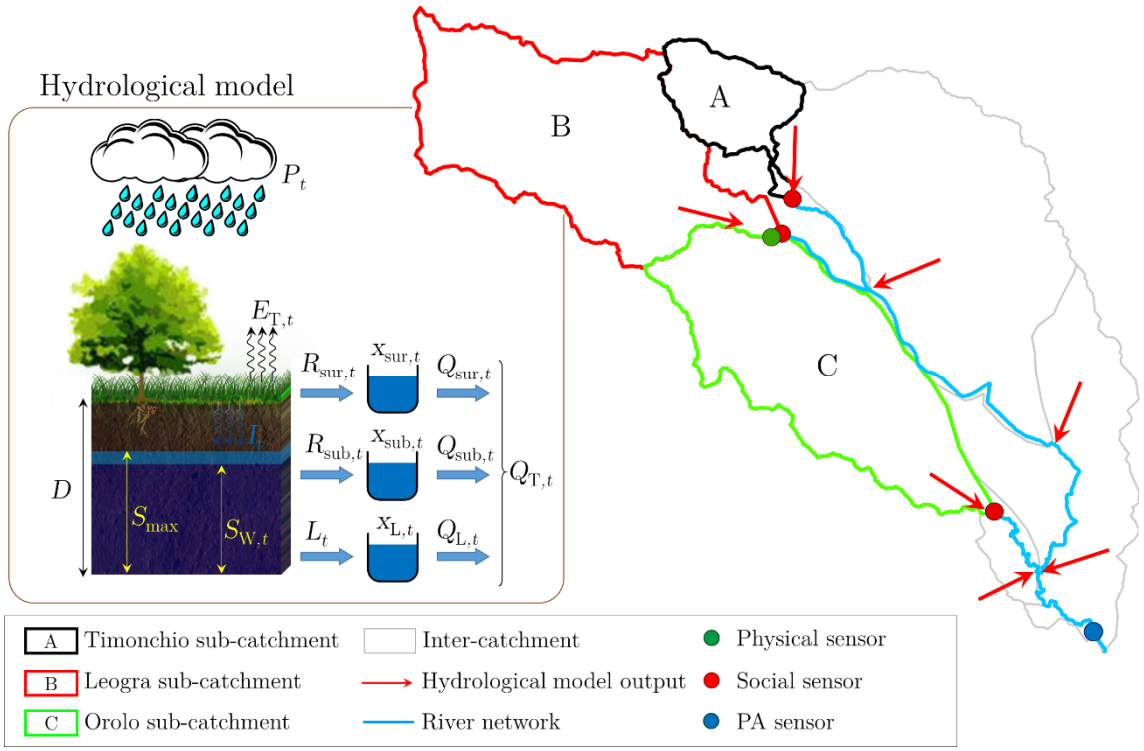

1003

1004 Figure 2. Structure of the early warning system AMICO and location of the physical, social and
1005 Ponte degli Angeli (PA) sensors implemented in the Bacchiglione catchment by the Alto
1006 Adriatico Water Authority

1007

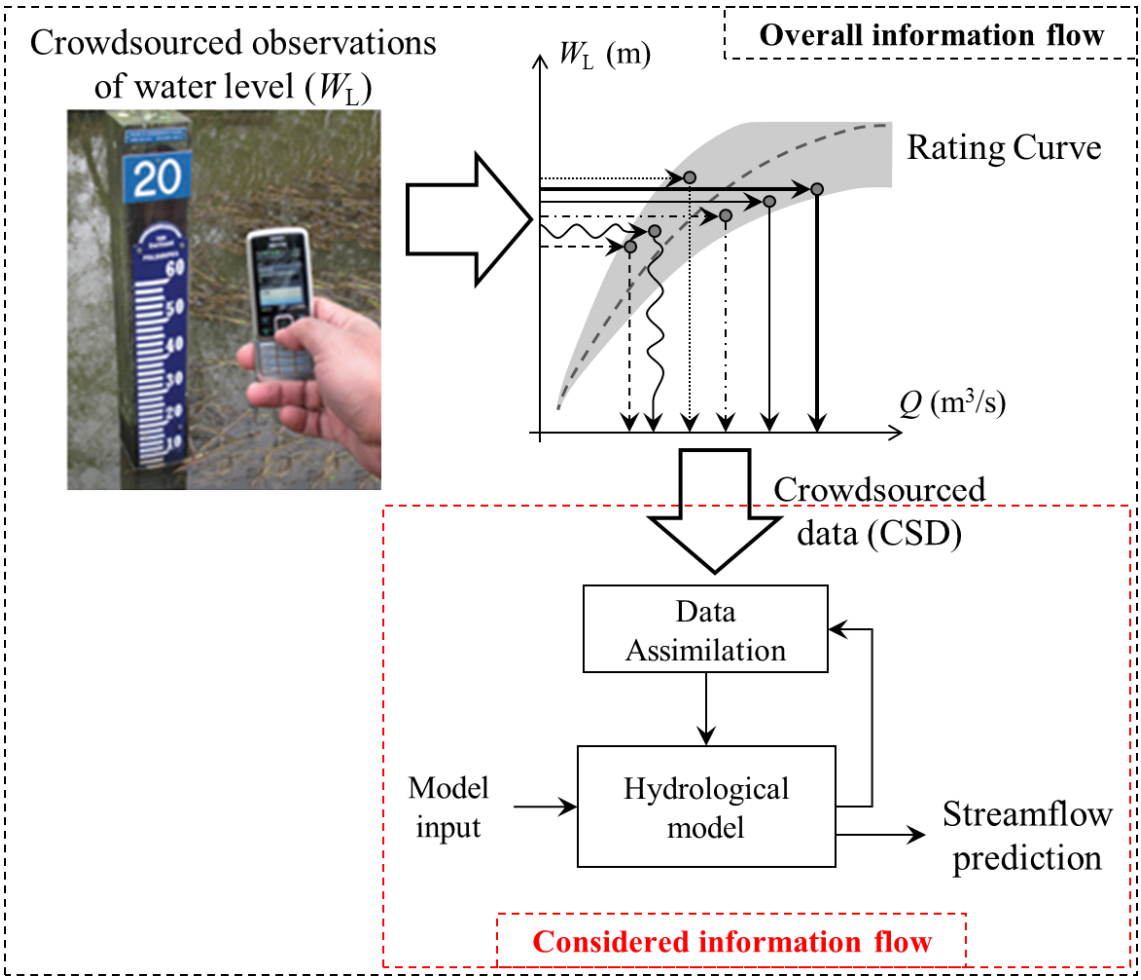

Figure 3. Graphical representation of the methodology proposed to estimate crowdsourced data of streamflow from crowdsourced observations of water level and then assimilate them within hydrological model

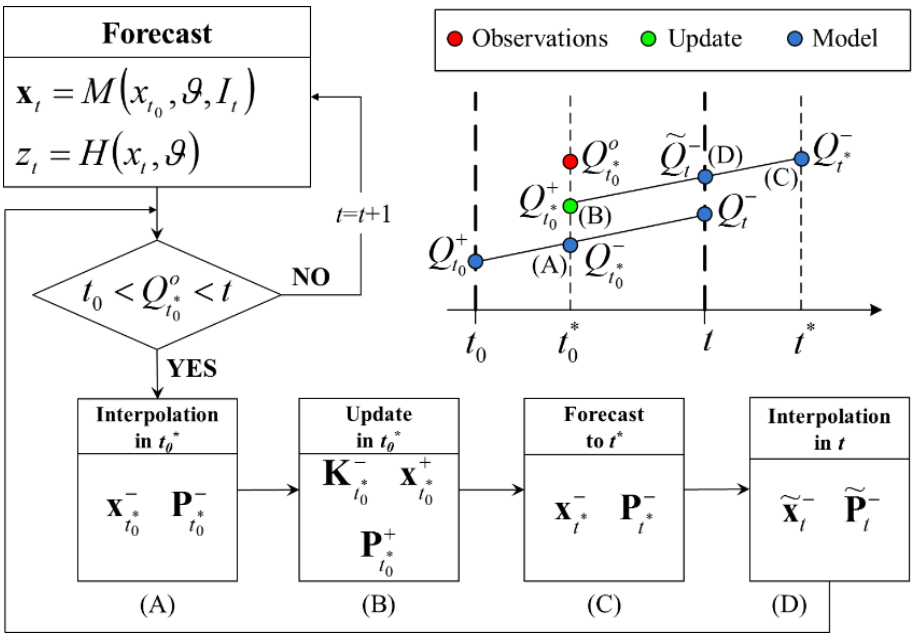

Figure 4. Graphical representation of the DACO method proposed in this study to assimilate asynchronous CSD

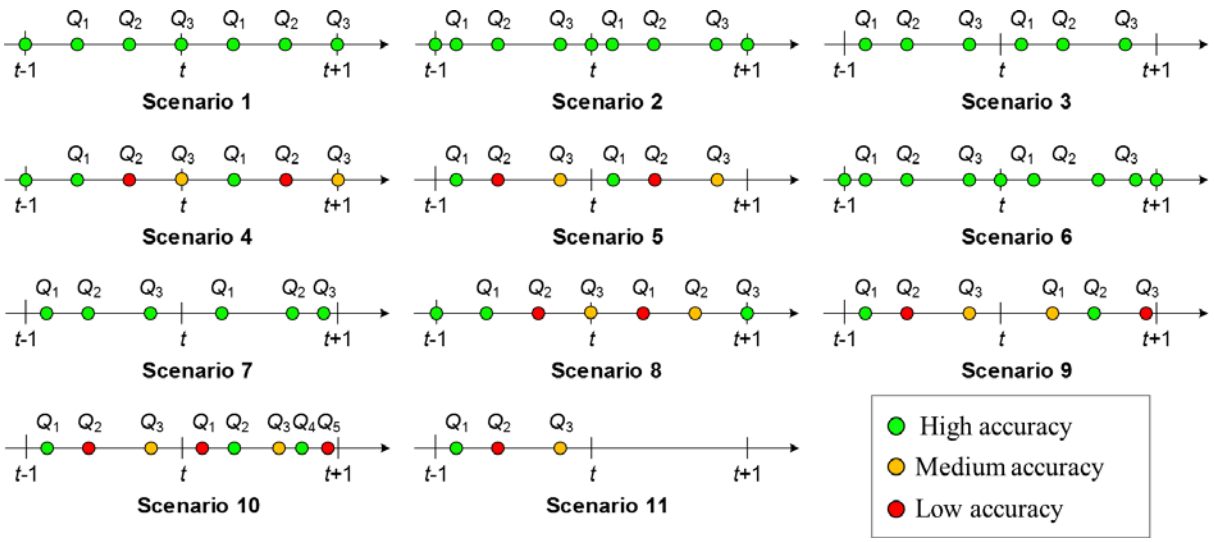

Figure 5. The experimental scenarios representing different configurations of arrival frequencies, number and accuracies of CSD

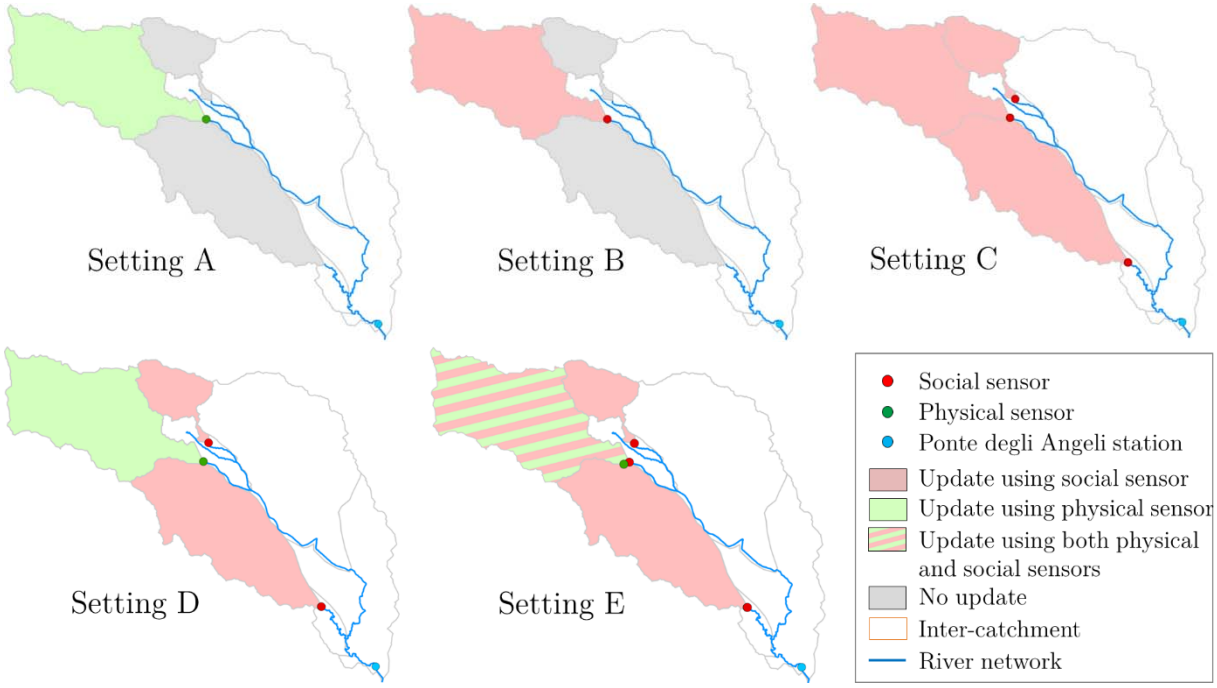

Figure 6. Different experimental settings implemented within the Bacchiglione catchment during Experiment 2

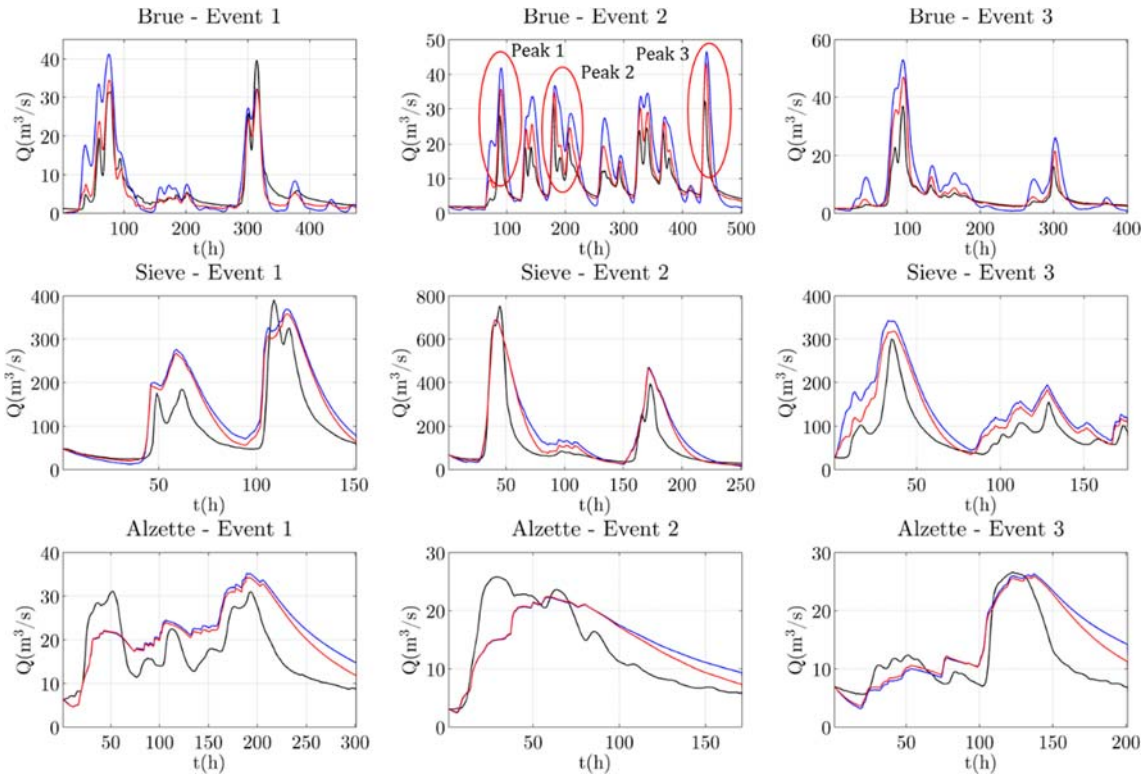

Figure 7. The observed and simulated hydrographs, with and without assimilation, for the nine considered flood events occurred in the Brue, Sieve and Alzette catchments

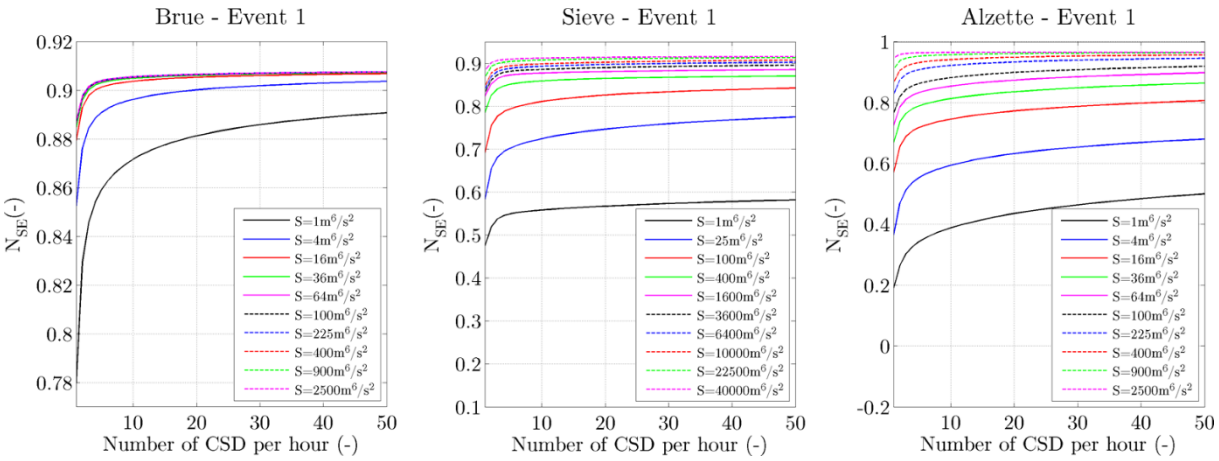

Figure 8. Model improvement in terms of N_{SE} during flood event 1 of each case study, for different values of model error matrix **S** and 24-h lead time, assimilating streamflow CSD according to scenario 1

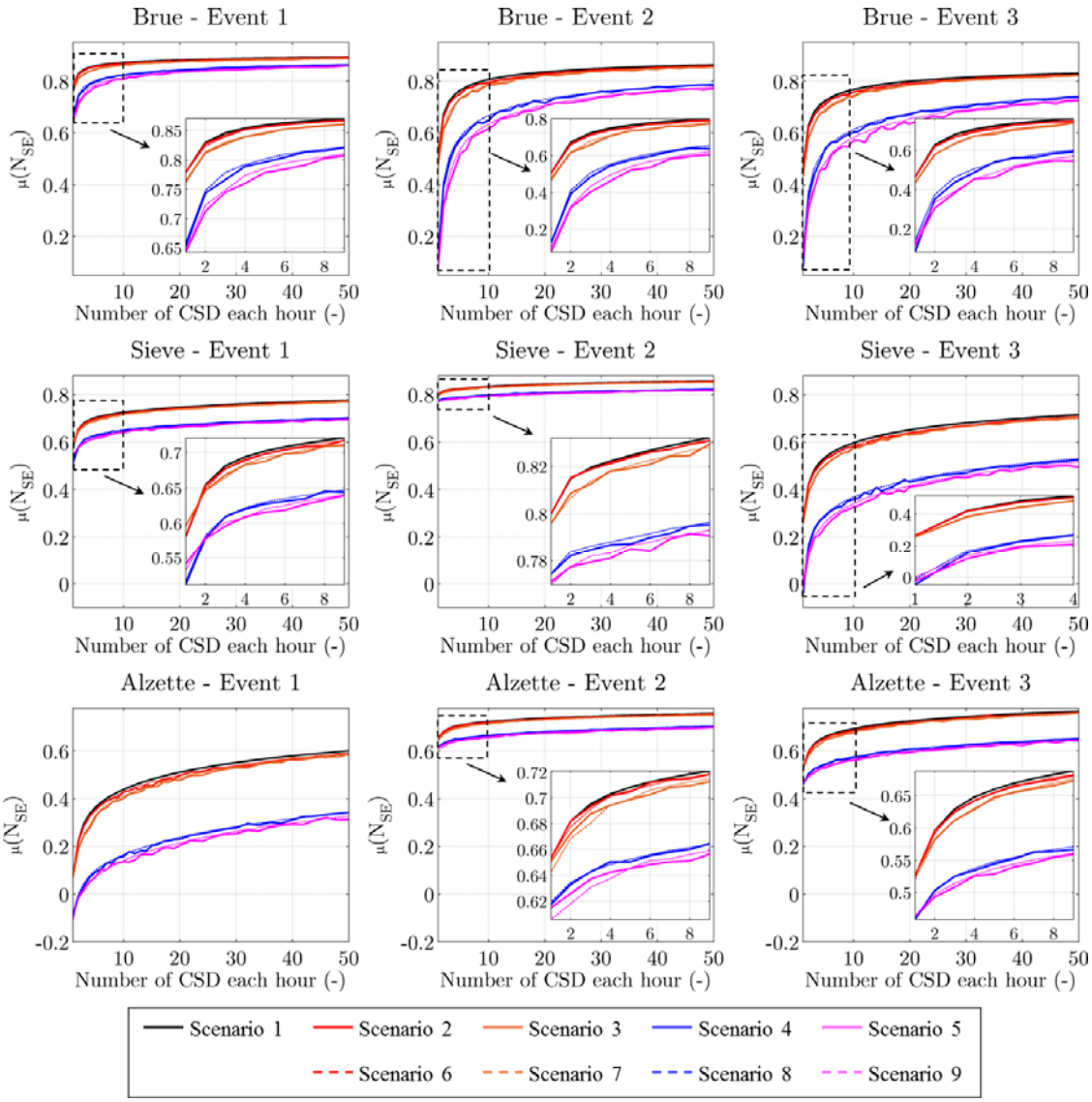

Figure 9. Dependency of mean of the N_{SE} sample, $\mu(N_{SE})$, on the number of CSD, for the scenarios 2, 3, 4, 5, 6, 7, 8 and 9 for the five considered flood events

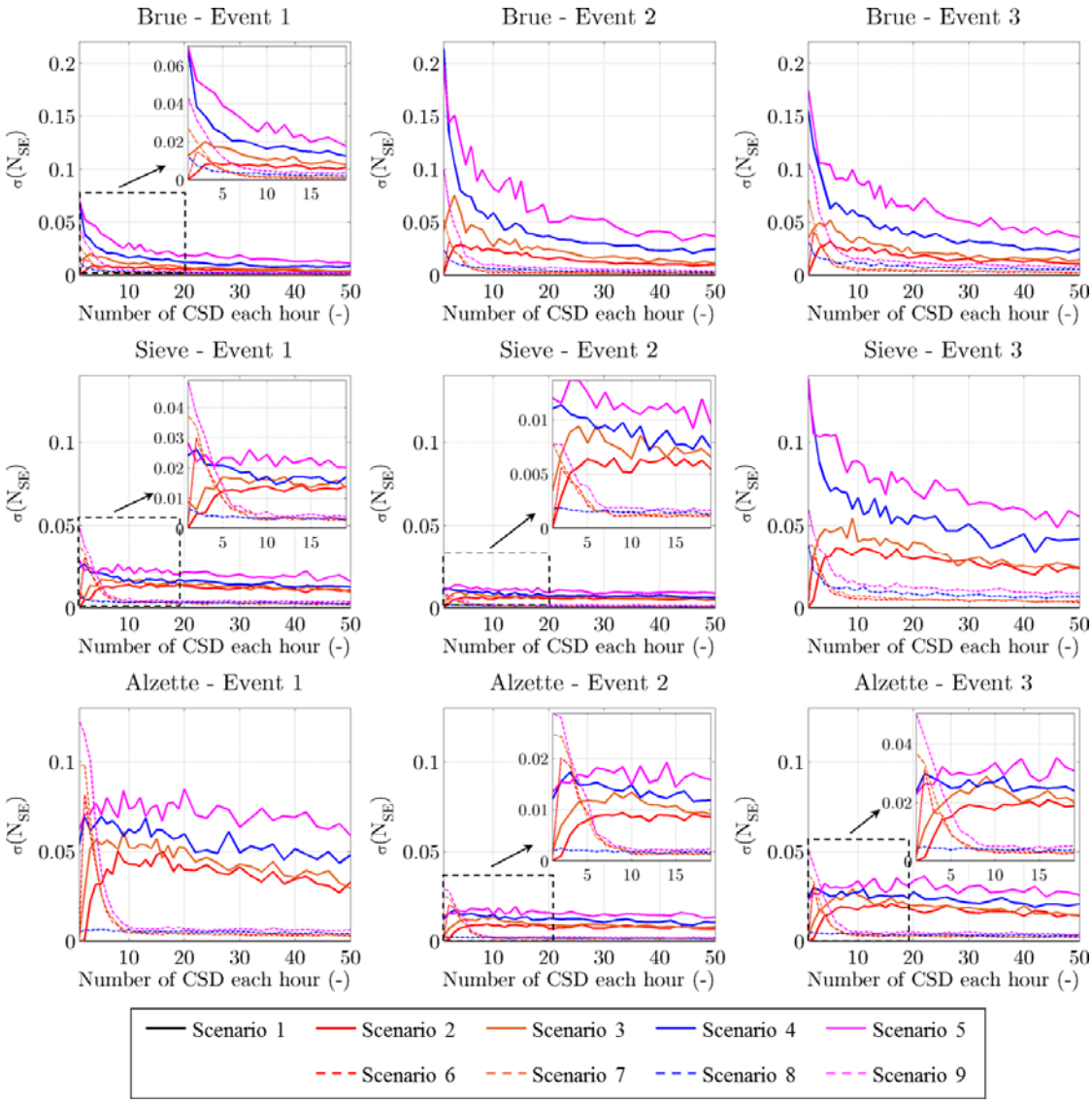

Figure 10. Dependency of standard deviation of the N_{SE} sample, $\sigma(N_{SE})$, on the number of CSD, for the scenarios 2, 3, 4, 5, 6, 7, 8 and 9 for the five considered flood events

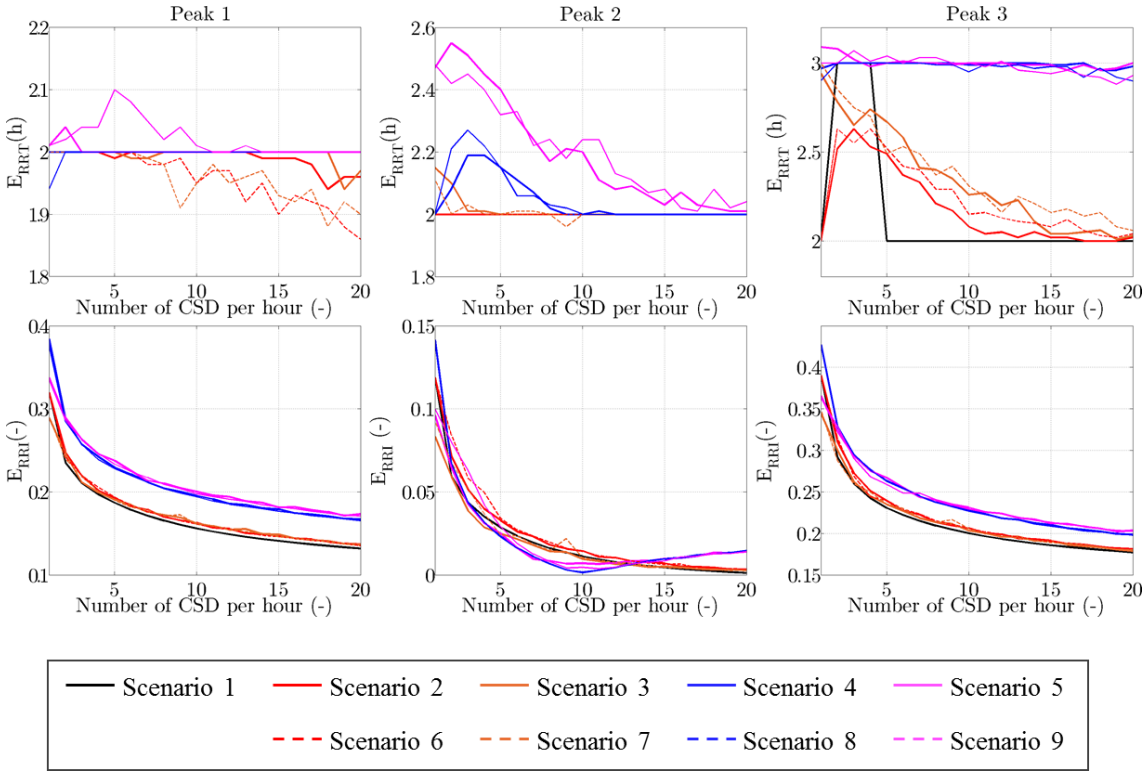

Figure 11. Representation of the E_{RRT} and E_{RRI}, described in Eqs. (20) and (21), as function of number of CSD and experimental scenarios for three different flood peaks occurred during flood event 2 in Brue catchment

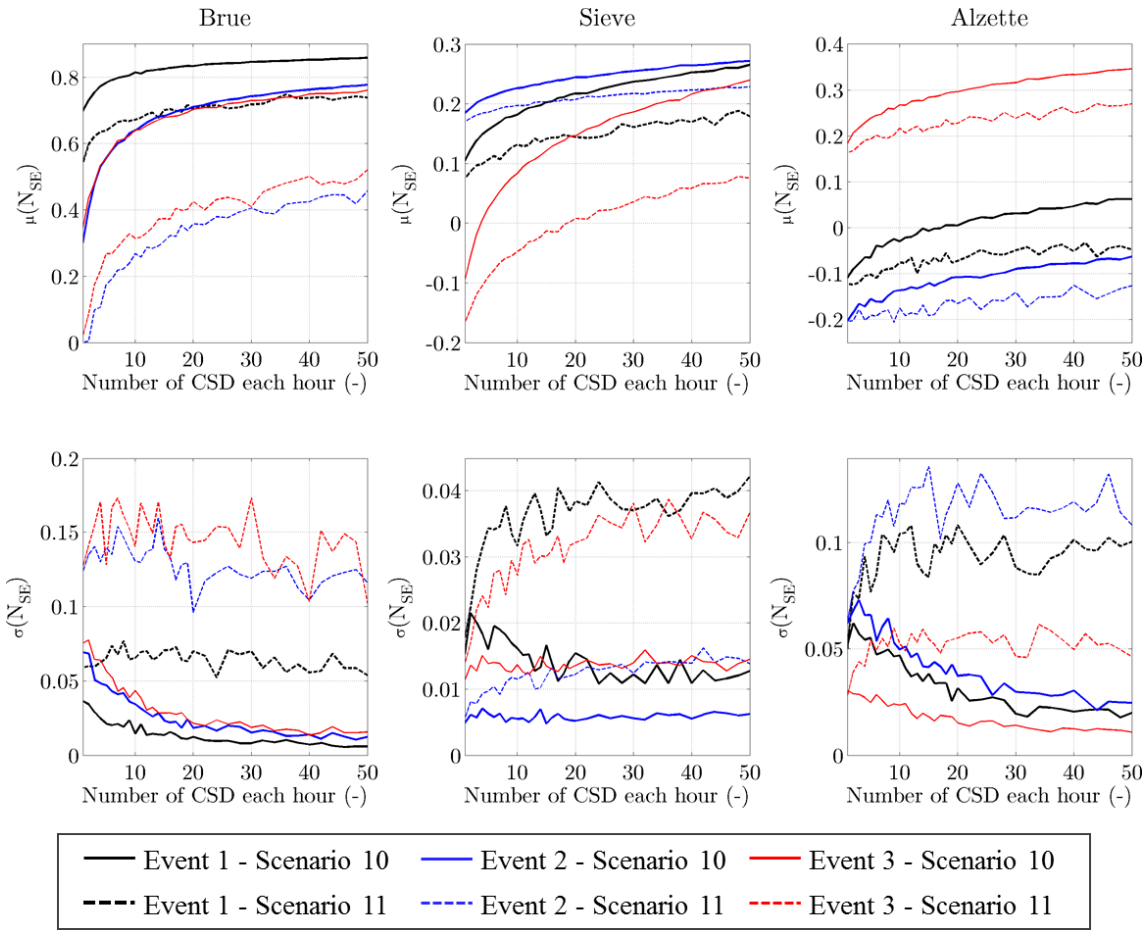

Figure 12. Dependency of the $\mu(N_{SE})$ and $\sigma(N_{SE})$ on the number of CSD, for the scenarios 10 and 11 for the five flood events

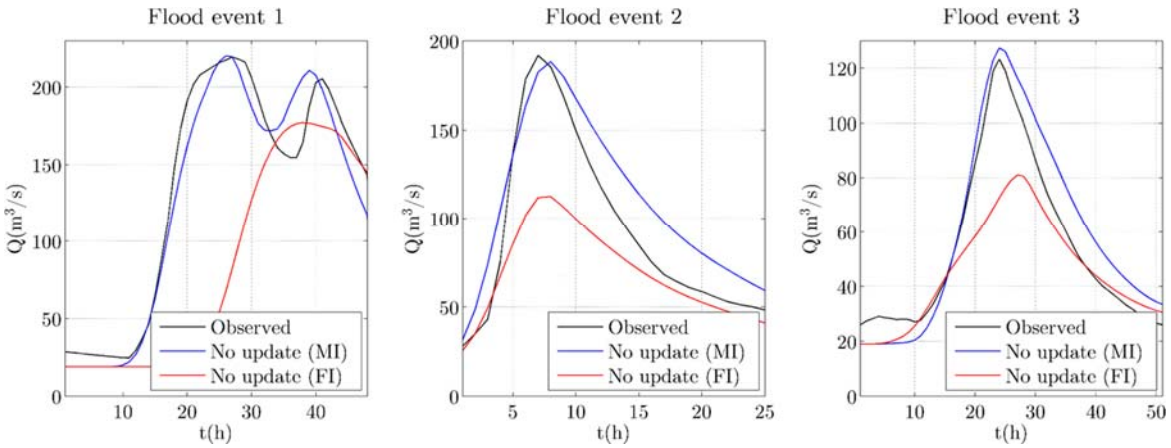

Figure 13. The observed and simulated hydrographs, without update, using measured input (MI) and forecasted input (FI), for the three considered flood events occurred in 2013 (event 1), 2014 (event 2) and 2016 (event 3) on the Bacchiglione catchment

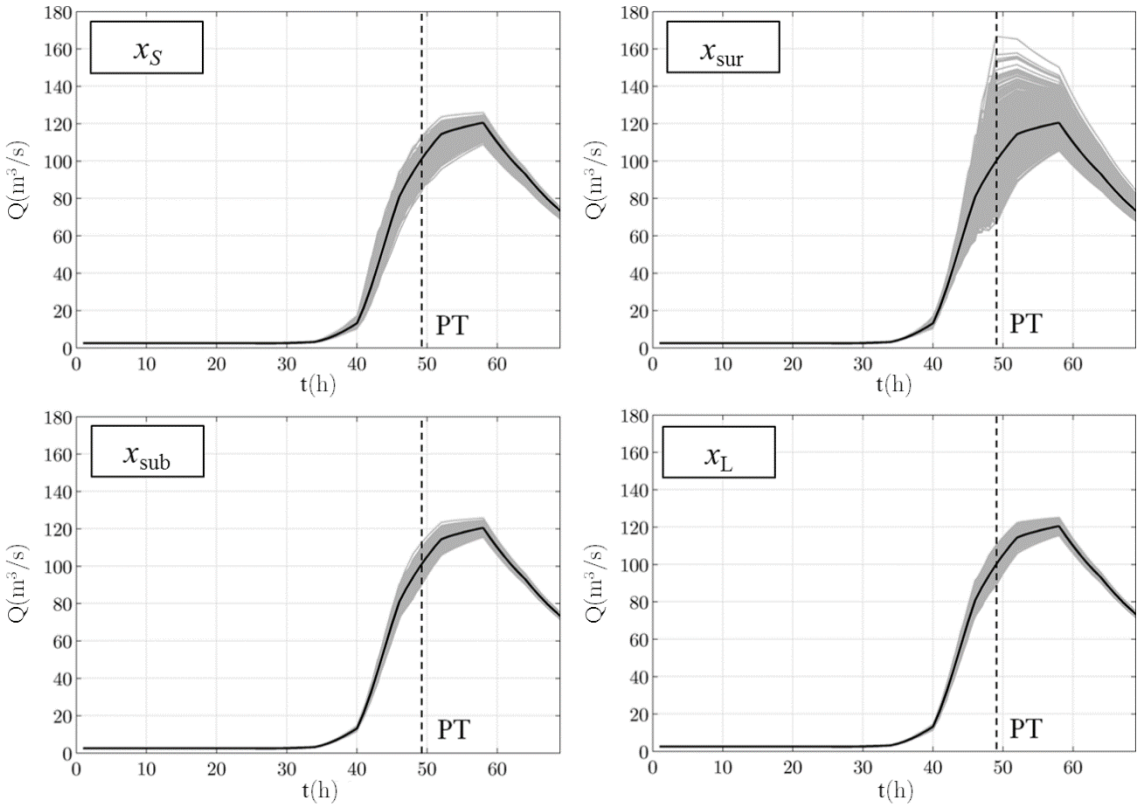

Figure 14. Effect of perturbing the model states on the model output, Bacchiglione case study. PT=Perturbation Time

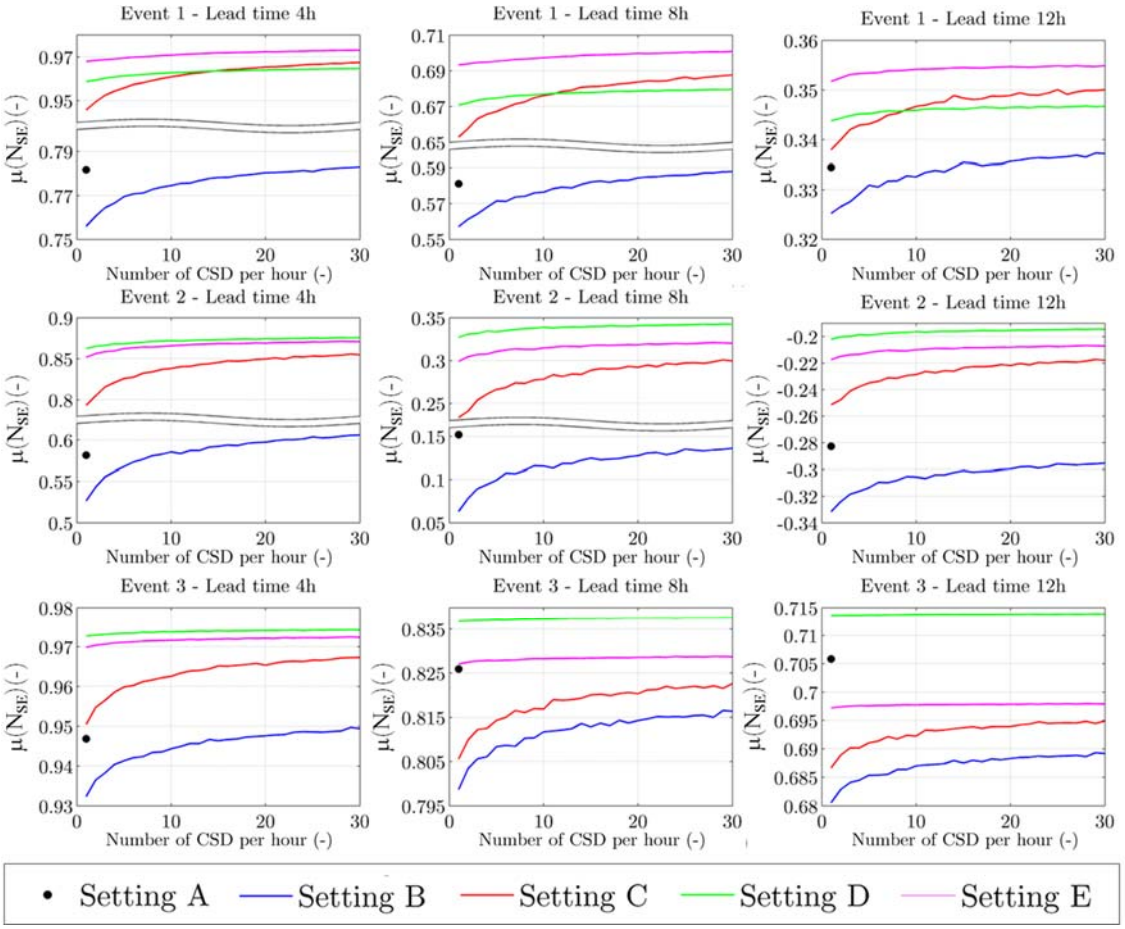

1063

1064 Figure 15. Model performance expressed as $\mu(N_{SE})$ – assimilating different number of CSD
1065 during the three considered flood events, for the three lead time values, having characteristic of
1066 scenario 10

1067

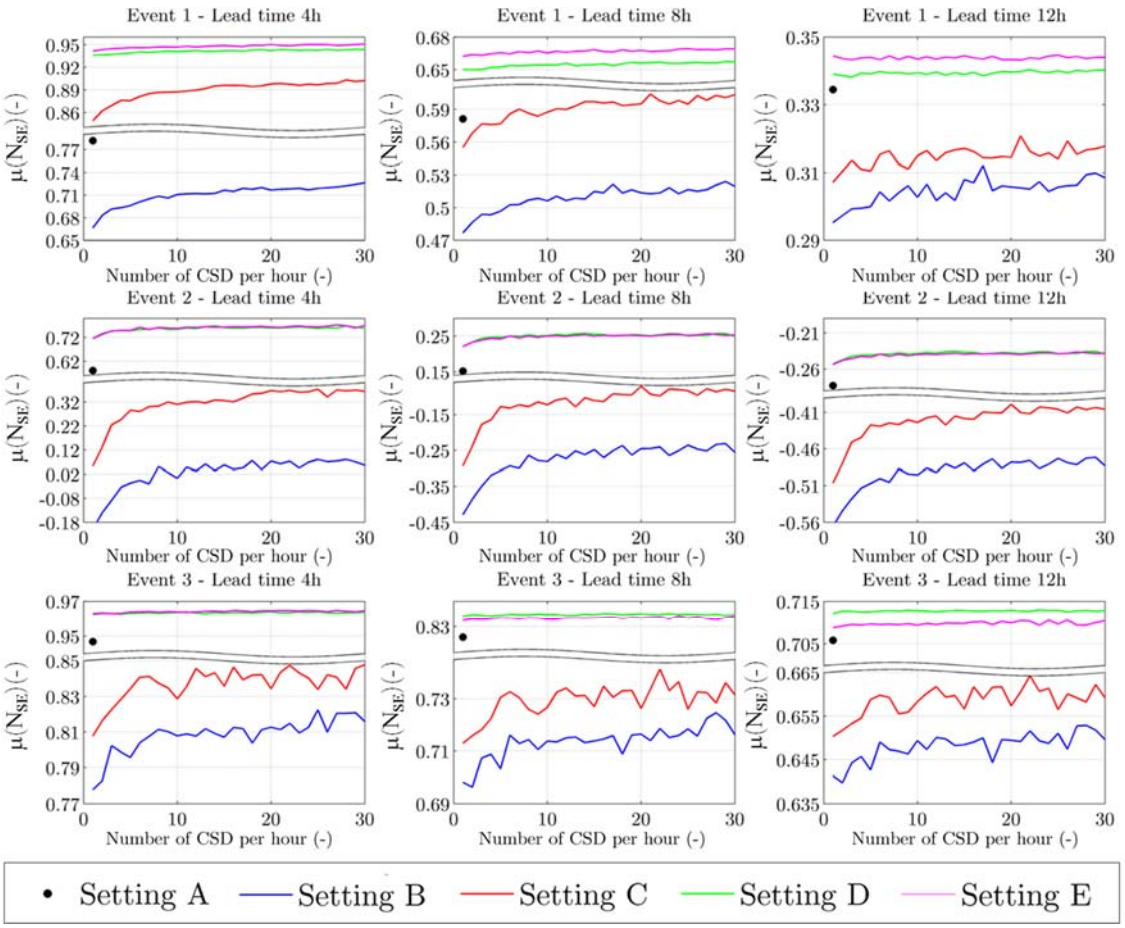

Figure 16. Model performance expressed as $\mu(N_{SE})$ – assimilating different number of CSD during the three considered flood events, for the three lead time values, having characteristic of scenario 11

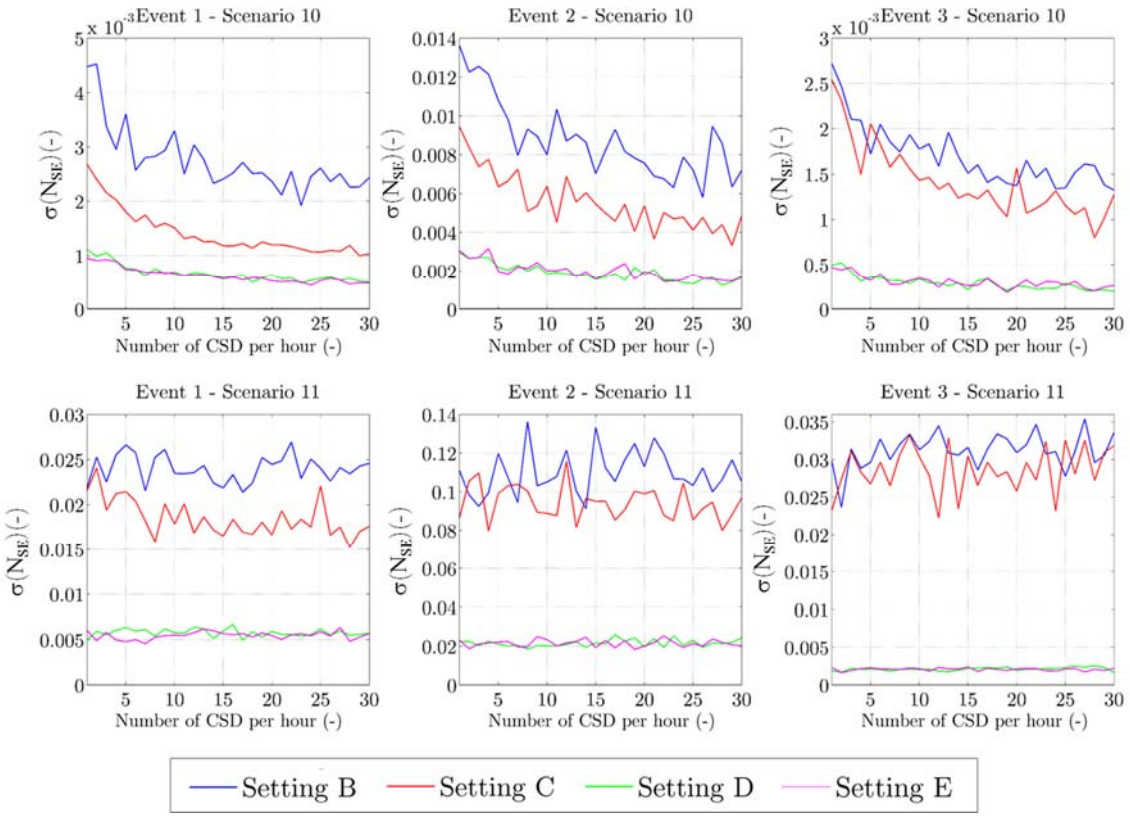

Figure 17. Variability of performance expressed as $\sigma(N_{SE})$ – assimilating CSD within settings A, B, C and D, assuming the lead time of 4h, for scenarios 10 and 11 during the three considered flood events